NASA CONTRACTOR REPORT

PARTICLE ACCELERATION BY EVAPORATION PRESSURE

by R. F. Wuerker

Prepared by
TRW SYSTEMS
Redondo Beach, Calif.
for Manned Spacecraft Center

NATIONAL AERONAUTICS AND SPACE ADMINISTRATION • WASHINGTON, D. C. • NOVEMBER 1967

PARTICLE ACCELERATION BY EVAPORATION PRESSURE

By R. F. Wuerker

Issued by Originator as Report No. 04848-6001-R0-000

Prepared under Contract No. NAS 9-5113 by
TRW SYSTEMS
Redondo Beach, Calif.

for Manned Spacecraft Center

NATIONAL AERONAUTICS AND SPACE ADMINISTRATION

For sale by the Clearinghouse for Federal Scientific and Technical Information
Springfield, Virginia 22151 – CFSTI price $3.00

FOREWORD

The following study on the feasibility of accelerating particulate matter to meteoric velocities with the focused radiation from a megawatt pulsed laser system was undertaken by Drs. L. O. Heflinger and R. F. Wuerker at the Physical Research Center of TRW Inc., Redondo Beach, California. The final report was authored by R. F. Wuerker except for Appendices I and III which were authored by L. O. Heflinger. Laboratory assistance was provided by R. A. Briones.

The investigators want to acknowledge the assistance and fruitful discussions with C. Knox and A. V. Haeff of this laboratory.

TABLE OF CONTENTS

CHAPTER I
ELEMENTARY CONSIDERATIONS AND PROGRAM SCOPE

INTRODUCTION

High intensity lasers offer in principle a new approach to the acceleration of matter to high velocities. The technique is that of using the focused radiation from a pulsed solid state laser system to ablate one side of a small particle and thereby impart momentum to the remaining mass.[1,2] The study reported herein has been concerned with the feasibility of accelerating particles of the order of 100 microns in diameter to meteoric type velocities of the order of 20 kilometers per second via laser induced ablation.

THE ROCKET EQUATION

Close analogy can be drawn between the acceleration of a particle by the focused radiation from a pulsed solid state laser and the acceleration of a rocket by the expulsion of propellant by fuel carried in the rocket. The basic difference between the two approaches is the fact that the rocket carries its source of energy, while in the laser acceleration system the energy is electromagnetically transmitted to the particle. In each case the rocket equation is strictly applicable; namely,

$$M_f = M_i - \Delta = M_i \exp\{-v_f/C\} \quad ; \quad \text{I-1)}$$

where,

M_f is the final mass after burn out,

M_i is the initial mass,

Δ is the mass ablated (propellant mass),

v_f is the final velocity of the remaining mass (M_f),

and

C is the effective exhaust velocity.*

---

[1] G. A. Askaryan and E. M. Moroz, J. Exp. Theor. Phys. (U.S.S.R.) 43, 2319-2320 (1962)

[2] S. Altshuler, "Laser Particle Accelerator," TRW Invention Document #843, February 1963.

*The effective exhaust velocity C is the average of all of the particles expelled by the burning process which transfer forward momentum to the remaining mass.

The consequences of the rocket equation are shown by the numerical values compiled in Table I. Clearly demonstrated is the major truism; namely, that terminal velocities in excess of the effective exhaust velocity require the consumption of the major fraction of the original particle mass.

TABLE I-1
NUMERICAL VALUES OF THE ROCKET EQUATION

Ratio of final velocity to effective exhaust v_f/C	Ratio of final mass to initial mass M_f/M_i	Ratio of initial mass to mass ablated M_i/Δ	Ratio of effective exhaust velocity to final velocity C/v_f
0.2	0.8187	5.5167	5.0
0.3	0.7408	3.8583	3.33
0.4	0.6703	3.0332	2.5
0.5	0.6065	2.5415	2.0
0.6	0.5488	2.2164	1.66
0.7	0.4966	1.9864	1.43
0.8	0.4493	1.8160	1.25
0.9	0.4065	1.6851	1.11
1.0	0.3679	1.5820	1.0
1.5	0.2231	1.2872	0.66
2.0	0.1353	1.1565	0.5
2.5	0.0821	1.0894	0.4
3.0	0.0498	1.0524	0.33
4.0	0.0183	1.0187	0.25
5.0	0.0067	1.0068	0.2

Stated more practically, the final velocity of a rocket can approach its exhaust velocity, but for a rocket to exceed its exhaust velocity by a factor of two requires essentially its complete consumption. These facts are clearly illustrated by the values tabulated in Table I. A linear plot of the ratio of the effective exhaust velocity to the final velocity (fourth column) versus the ratio of initial mass to mass ablated (third column of Table I) is, as can be seen in Figure I-1(for values of $M_i/\Delta \gtrsim 1.5$), essentially a curve of unity slope with intercepts at $M_i/\Delta = 1/2$ and $C/v_f = -1/2$. The asymptotic form of the curve can be illustrated by recasting the rocket equation in

less familiar form; namely,

$$\frac{C}{v_f} = \frac{-1}{\ln\left(1 - \frac{\Delta}{M_i}\right)} \qquad \text{I- 2)}$$

and expanding (for small Δ), the right hand side in a power series; one obtains,

$$\frac{C}{v_f} = \frac{Mo}{\Delta} - \frac{1}{12} - \frac{1}{12}\left(\frac{\Delta}{Mo}\right) + \cdots \qquad \text{I- 3)}$$

The plot shown in Figure 1 emphasizes the linear nature of the rocket equation when the ablated mass is not the major fraction of the initial mass. Conversely, when the final velocity is around twice the effective exhaust velocity, a rocket is operating highly non-linearly.

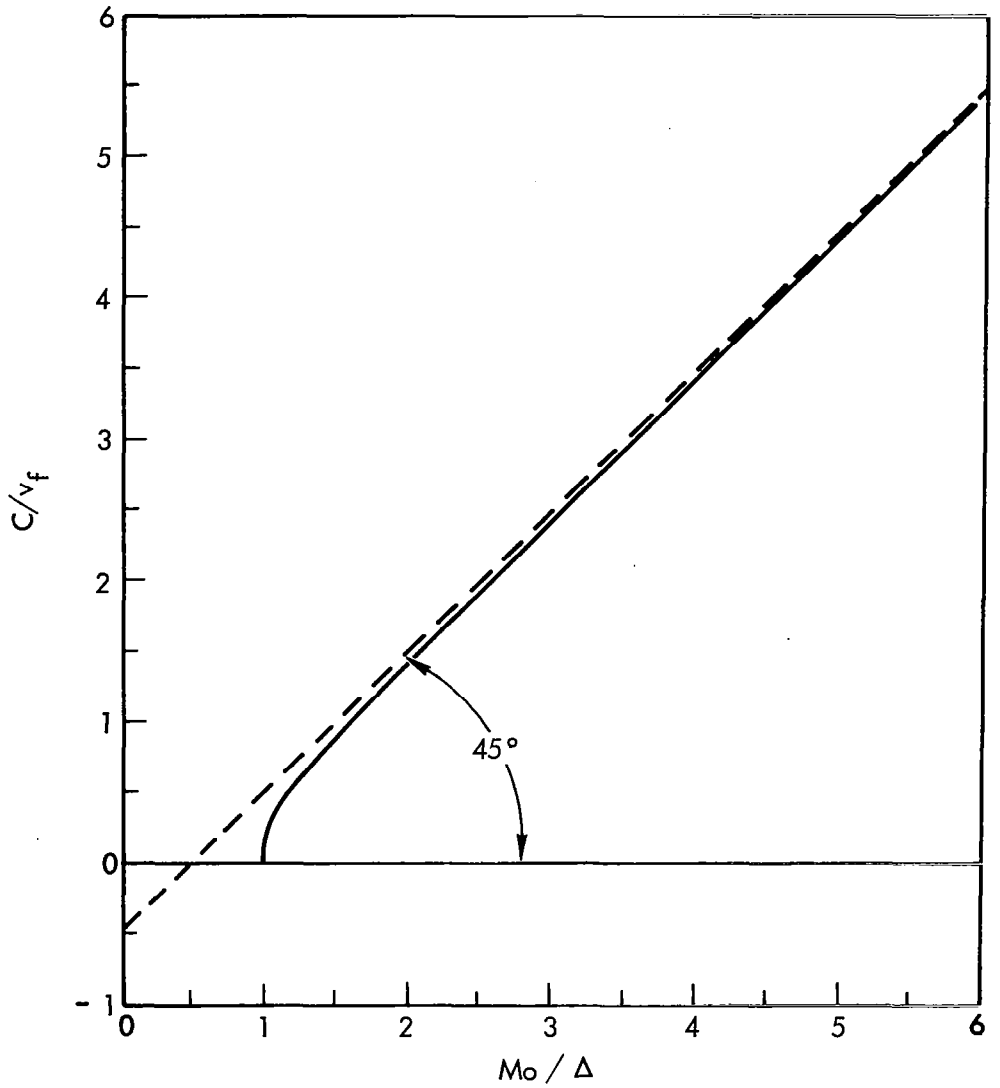

Figure I-1 Normalized Plot of Rocket Equation showing ratio of effective exhaust velocity to final velocity versus ratio of initial mass to mass ablated.

THE EXPERIMENTAL PROGRAM

The previous section emphasized that the ultimate feasibility of the pulsed laser approach to the acceleration of small particles of matter to meteoric velocities depends upon the effective exhaust velocities which can be realized when the radiation from a laser is focused onto the surface. Stated another way, the effective exhaust velocity determines the upper velocity to which a particle can be accelerated with a laser.

Other questions (such as, whether the particle or material has sufficient strength to withstand the mechanical forces of the laser induced evaporation, whether it can be kept in the laser beam,* etc.) are all of secondary importance compared to the question of the magnitude of the effective exhaust velocity which can be realized by a focused beam of electromagnetic energy.

Since feasibility was so dependent upon the effective exhaust velocity, the program concentrated almost exclusively upon the accurate measurement of this quality. As time went on, the technique was refined until by the end of the program reliable measurements of exit velocity were being made on particles in the size range of interest to the program.

The determination of effective exhaust velocity is in principle straightforward; i.e., one measures the impulse delivered to a specimen or particle by the pulsed laser system and then divides this quantity by the mass lost.

Impulse can be measured in a variety of ways. One of the oldest and best techniques is that of measuring the stroke of a ballistic pendulum; namely,

$$\text{Impulse} = \int F dt = \frac{2\pi M_p X}{T} \qquad \text{I-4)}$$

where M_p is the mass of pendulum, bob

T is the period of the pendulum,

and X is the stroke or peak amplitude of oscillation

*The original TRW proposal for this work dealt with the problem and techniques of focusing the radiation over long distances via either calcite-variable-focus-lenses or by capillary tube (see TRW Proposal #4848.000, February 1965). In brief it was discovered that a glass capillary of typically 2.0 millimeters bore and 7.5 centimeter length would transmit 45% of a kv, 20 joule ~1/2 millisecond, 1.06 micron laser beam. The capillary thus looked like a very promising launcher.

Another approach is to freely accelerate a particle of known initial mass and to determine its final velocity. Further, if the final mass is also known, then the effective exhaust velocity is calculated directly from equation 1.

The ballistic pendulum approach was the technique used at the inception of this program. It has the advantage that its sensitivity for small impulses can be made high and that it requires a minimum of equipment. Once set up, samples can be routinely checked, etc. Its major problem is that measurements were most easily done on samples of large cross-sectional area (compared to the 100 micron size of interest) and that such measurements are weak due to the fact that one has no assurance that the impulse for flat plates is the same as that for small samples of the same size as the focal size of the laser.* Furthermore, since the mass of the samples are generally large, one has the problem of accurate measurements of small mass changes.

The free acceleration technique is preferred, particularly when one deals with particles of the size of interest to the goals of the present program. It is complicated by the fact that a 100 micron sized particle has a weight of approximately 20 micrograms and that the error in the determination of the effective exhaust velocity (by equation 1) is equal to error in the measurement of the mass ablated. For a 2 microgram mass loss, the measurement of the effective exhaust velocity to 10% requires a sensitivity of 0.2 microgram in the mass measuring apparatus. Mass measurement to such a degree of precision is generally beyond the capability of any of the commercial microbalances.

Suffice it to say that the free acceleration approach, with the mass of particle measured both before and after acceleration to an accuracy of 10%, was the approach finally adopted and developed. Its implementation required the perfection of a particle weighing device with 0.1 microgram

*Ballistic pendulums were used with wire samples mounted in the bob. The wires proved difficult to hit squarely on the tip with the focused laser beam due to the always present oscillation of the bob. The wire tipped pendulum technique could be criticized in addition from the point of view that the long length of wire served as a sink for acoustic energy deposited in the sample by the laser. Such energy could not escape from a microscopic particle. Experiments in the early part of the program were encouraging due to the fact that wires ~10 mills in diameter could be bent by the impact from a Q-switched laser.

sensitivity. The description of this unique reed mass measuring apparatus is described in detail separately in this report (see Appendix I). The experimental approach (which took the better part of the program to perfect) consisted of taking the test particle and weighing it with the reed vibrator to determine its initial mass (i.e., M_i). The weighed particle was then transferred to a lacquer film (~1/2 microns thick) stretched over a hole in an aluminum frame. The particle and frame were then placed in a small vacuum chamber (with replaceable plexiglas windows) attached to a commercial micromanipulator. The opposite end of the chamber mounted a lead zirconate piezoelectric crystal with a paraffin coating over the end face. While the chamber was being evacuated the particle was manipulated before the cross hairs of the telescope sighted to the laser beam.* When evacuation was complete, the laser was fired and the flight of the test sample from the mounting point to the piezoelectric crystal was monitored with an oscilloscope. The velocity of the particle (i.e., v_f) was computed from the known separation of the mounting frame and the piezoelectric crystal (typically 8-10 centimeters) and from the transit time measured from a photograph of the oscilloscope sweep (see Figure 7-IA in Appendix I).

The chamber was then refilled with air and the piezoelectric crystal removed and placed under an examining lamp. The impacted particle or fragment was then located and extracted from the paraffin coating with a pair of short tweezers. Excess paraffin was removed by soaking the recovered fragment in a trichlorobenzene solvent. The sample was then weighed (for the second time) with the vibrating reed apparatus and the final mass determined i.e., M_f). The effective exhaust velocity could then be computed directly from equation 1.

The approach outlined above gave experimental values for the true effective exhaust velocities generated by the impact of laser radiation on small particles. The values so determined were the mechanically measured values and were free of scaling problems, geometrical effects, etc.

*The laser was sighted by placing a sheet at the focal point of the concentrating lens and firing the laser. The cross hairs of the telescope were then leveled onto the impact site.

In summary, the program began quantitatively with measurements of laser produced impulses using vacuum mounted ballistic pendulums. These preliminary measurements at least roughly demonstrated which (out of all of the inorganic compounds of nature) yielded the highest impulse. The early measurements clarified the need for precision mass loss measurements and the need to conduct these measurements on particles of the same size as those of interest. The need resulted in the perfection of the reed vibrator for absolute measurement of particle mass in the 100 - 10μgram range to a precision of 10%. The program as enumerated in previous paragraphs was finally adopted and employed.

This was not an easy program; in general, it did not have the scope for the type of study one would ideally like to have had. In addition to the need for accurate measurements of impulse and mass loss on a wide variety of materials, the program was faced with the maintenance, operation and perfection of a Q-switched ruby laser oscillator and power amplifier system as well as an intermediate pulse (~50 microsecond) duration laser oscillator driven by a high current annular lamp. Both of these systems are described in detail in Appendix II of this report. In addition, there existed a wide variety of theory and experimental results by others of indirect measurements on the laser ablation of matter (i.e., plume front velocities, ion energies, electron energies, etc.). The latter measurements indicated that the plume had exhaust velocity components far in excess of the 20 kilometer speeds of interest to the present program.[2,3,4] These results, on the other hand, did not sense either the slower or non-ionized components of the plume and, as a result were meaningless as per questions concerning applicability of the laser technique to the acceleration of matter.

The following secions will describe in more detail the results and techniques of the laser acceleration program.

---

[2] J. F. Ready, "Development of Plume of Material Vaporized by a Giant Pulse Laser," Applied Physics Letter, Volume 3, pp. 11-13 (1963)

[3] W. I. Linlor, "Ion Energies Produced by Laser Giant Pulse," Applied Physics Letters, 3, 210-211 (1964)

[4] W. I. Linlor, "Some Properties of Plasma Produced by Giant Laser Pulse," Physical Rev. Letters, 12, 383 (1964)

CHAPTER II

PRELIMINARY MEASUREMENTS

The experimental investigations on this program were actually begun during the preparation of the initial proposal to the NASA/Manned Spacecraft Center. At that time a "conventional" half-millisecond duration laser with a 5/8" diameter x 8" long neodymium doped American Optical glass rod was set upon an optical bench along with the focusing optics and a telescopic sighting system.* A small ballistic pendulum consisting of a 3 centimeter long, 135 milligram capillary test tube was suspended by four 0.6 mill nylon thread before the focal point of the concentrating optical system. Test samples were placed in the bob of the pendulum and then precisely focused at the impact site of the laser. The impulse sensitivity of the bob could be controlled by adding mass to the bob (see Equation I-4). A photograph of this first very early setup is shown in Figure II-1. Simple results of first measurements of effective exhaust velocity are presented in Table II-1 for 1/32-inch diameter test samples of aluminum, tungsten, iron (drill rod), and graphite pencil lead. The rods were weighed on a Mettler Model M-5 microbalance ($\pm$ 10 microgram sensitivity) in order to monitor the amount of test material ablated by the laser impact. The results clearly indicate that the conventional 1/2 millisecond duration spiking laser produces too low of an effective exhaust velocity with metal targets. Carbon (i.e., pencil lead)

*The laser rod had a TIR or corner reflector on one end and a plane uncoated surface on the other end. The laser cavity was formed with an external ~55% plane dielectric coated mirror. The output beam was characterized by a low degree of beam divergence. The emission could be finely focused, for example, with a 6.5 cm focal length lens. This laser would puncture through 0.10 inch thick steel in a single pulse. With a single element x 4 microscope objective, an integrated emission of 6.8 joules would produce a 300 micron diameter hole in a 0.04 inch thick stainless steel plate, while 1.5 joules would produce 100 micron diameter holes in the same plate. An improved focusing system, namely, 6.5 centimeter lens acting as a relay for the x 4 objective, and 2.6 joules out, could produce 30 micron holes.

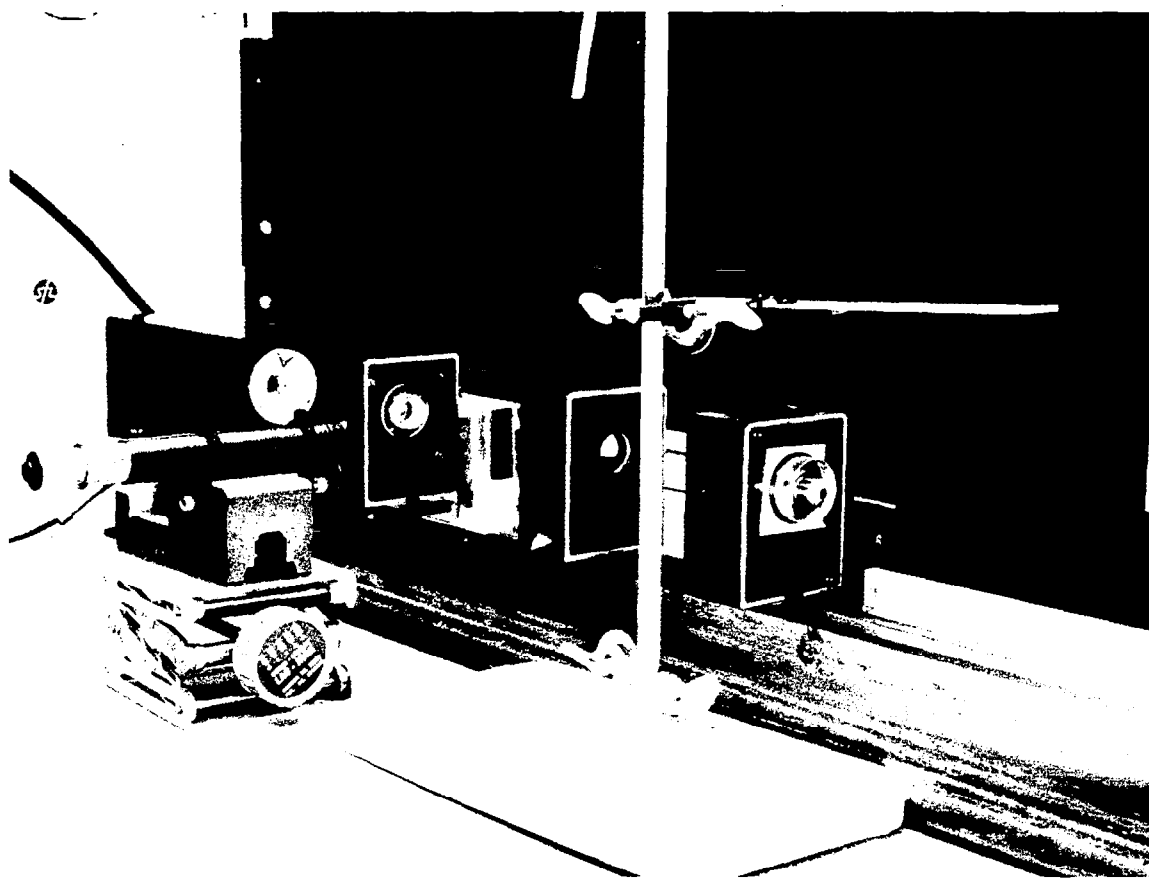

Figure II-1: Photograph of the first laser ballistic pendulum apparatus used at TRW Systems for measurement of the effective exhaust velocity produced by the focused laser radiation. The double lamp laser head, external dielectric end reflector, 6.5 centimeter relay lens, and an x 4 microscope objective were mounted on a common optical bench. Samples mounted in the ballistic pendulum were positioned at the focal point of the objective by a telescope focused for infinity which "looks" down the optical focusing system.

TABLE II-1

EFFECTIVE EXHAUST VELOCITIES MEASURED WITH 1/2 MILLISECOND NEODYMIUM LASER

Material	Sample Diameter Inches	Laser Emission Joules	Impulse via Ballistic Pendulum ~~Dyne-sec.~~	Mass Loss Milligrams	Effective Exhaust Velocity C Kilometer/sec.
W	0.030	1.5	0.70	0.16	0.045
W	0.030	2.5	1.95	0.28	0.070
W	0.030	6.5	4.8	0.67	0.075
Fe	0.045	1.5	3.2	0.38	0.084
Fe	0.045	2.6	3.0	0.55	0.060
Fe	0.045	6.5	10.2	1.00	0.102
Al	0.025	1.5	1.2	0.25	0.047
Al	0.025	2.6	3.5	0.40	0.090
Al	0.025	6.5	5.8	0.45	0.130
C	0.036	1.5	6.4	0.05	1.20
C	0.036	2.6	6.6	0.085	1.00
C	0.036	6.5	22.5	0.12	1.90

produced the highest exhaust velocity, but these values were too low to be of any particular interest. The focusing of a laser beam on a material surface is quite dramatic. Besides a loud report, the phenomena is in many cases characterized by an impressive pyrotechnic type of display. One soon learned that samples which emitted or ablated a large shower of sparks and trails were characterized by a high mass loss and hence a low effective exhaust velocity. The photographs shown in Figure II-2 are typical of the type of ablation observed when the output of a conventional (millisecond duration laser) is focused on matter. The pictures belong with the values presented in Table II-1, and were made with a conventional Polaroid camera with its shutter open during the impact of the focused neodymium radiation.

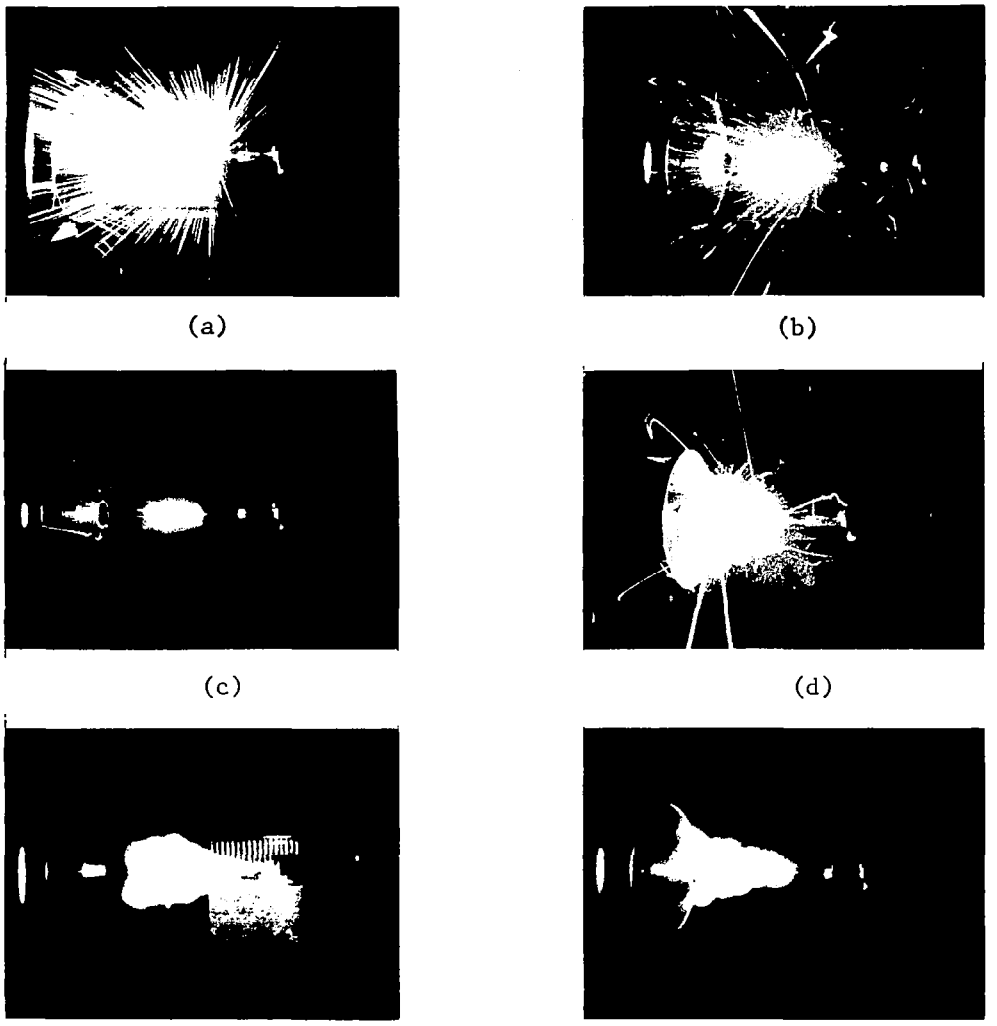

Figure II-2: Time integrated photographs of the ablation, Table II-1 samples, under focused beam from the neodymium laser system shown in Figure II-1.

a. Tungsten under 2.6 joule - 1/2 millisecond 1.06μ focused laser pulse

b. Carbon steel under 2.6 joule - 1/2 millisecond 1.06μ focused laser pulse

c. Aluminum under 2.6 joule - 1/2 millisecond 1.06μ focused laser pulse

d. Aluminum under 6.5 joule - 1/2 millisecond 1.06μ focused laser pulse

e. Graphite under 2.6 joule - 1/2 millisecond 1.06μ focused laser pulse

f. Graphite under 2.6 joule - 1/2 millisecond 1.06μ focused laser pulse

With the initiation of this contract, first experimental measurements of impulse and ablated mass loss were begun with the intermediate duration laser system. This unique laser was based upon a low inductance annular flash lamp of high mechanical strength and a low inductance 38,000 joule capacitor bank, the combination having a discharge time of ∿80 microseconds.* The laser system was developed under an Air Force Program (AF 33(615)-1072) and was designed to accept 5/8-inch diameter x 8-inch long solid state laser rods. The emission or lasing time of rods excited by this system were typically 20-40 microseconds, depending, of course, upon the particular laser rod. The intermediate laser system was of particular interest to the present program due to the fact that the emission times were of the proper order for the acceleration of 100 micron particles to velocities of 20 kilometers per second without exceeding the yield strength of the materials.**

At the start of this program the annular lamp was in a state of complete disassembly. It was accordingly completely rebuilt and in the process many improvements were added such as grounded shields around all of the high voltage lines, felt matting glued to the inside of the high voltage shields, and clay packing between all the cracks of the capacitor bank. The intent was to contain any shock wave generated by an accidental breakdown (due to insulator failure) of the charged capacitor bank. In addition, a heavy I-beam was added to the system so that external mirrors could be mounted before the laser rod mounted within the lamp.

The system was tested with a new 5/8-inch diameter by 8-inch long ruby rod specially ordered for the program. The rod was found to emit 24 joules at a capacitor bank loading of 29,500 joules (i.e., 4.5 KV - across 2,930μF). It was not of particularly high uniformity and as a result the emitted beam could not be finely focused.+

---

*The intermediate duration laser system is described in complete detail in Appendix II of this report.

**Appendix III in particular discusses the role of the proper acceleration time.

+Product of Linde Crystal Products Division (laser rod classified as S.I.Q. grade.

The ruby laser rod was replaced by a neodymium doped laser rod manufactured by American Optical Company. The emission from this rod was approximately the same as that of the ruby; however, due to the high homogeneity of the glass host the output could be much more sharply focused.

A small vacuum chamber in the shape of a plumbing "T" was fabricated from 3-3/4-inch inside diameter aluminum stock. The chamber was light enough and small enough so that it could be attached to a commercial micromanipulator. The chamber and vacuum pump were interconnected by a piece of reinforced Tygon tubing. The three open ends of the chamber were sealed by O-rings and Plexiglas plates. Plexiglas windows were chosen due to the fact that they could be replaced economically even on a shot to shot basis. Also, they were not prone to shatter like glass due to an unforeseen laser induced crack while the windows were supporting an atmosphere. A mechanical vacuum gauge was attached to the vacuum line along with an electronic Peroni vacuum gauge. The evacuation system was intended to remove air from the focal point of the laser beam and thereby prevent any breakdown effects from either dominating or influencing the laser interactions with the metal surface.

Small ballistic pendulums ($\sim$0.4 second period) were mounted in the vacuum chamber and the impulse of the laser induced damage was measured by the stroke of the pendulum.

Many materials were tested without measurement of impulse since it was generally appreciated by this time that for a given laser energy the impulse changed little from material to material, but that those materials which exhibited low mass loss were actually the ones of greatest interest to the possible acceleration of matter to hypervelocities. For impulses in the 50 dyne-second range, mass losses of less than 0.1 milligram had to be experienced before a given material was of any interest.

Ferrite material (density 5 gms/cm^3 in the form of a transformer core; see Appendix II, Figure 8-IIA) was found to lose 0.55 milligrams.

The crater was dish shaped ∿0.7mm diameter, 0.2mm deep (estimated) with a calculated mass loss of 0.4 milligrams. Boron nitride samples showed mass losses of 0.4 milligrams. Tungsten had mass losses of 0.9 milligrams per focused laser impact and showed a large number of streaks, indicating that a large fraction of material was being lost as superheated particulate matter.

The results of several experimental measurements are presented in Table II-2. For this set of data the exhaust velocity was determined from the impulse measured with the vacuum ballistic pendulum (sensitivity ∿35 dyne-second/cm deflection) and from "before and after" mass loss measurements with the Mettler balance.

The impulse was determined from the peak to peak stroke of the pendulum from equation I-4. To measure the stroke a pair of (1 microsecond duration) strobe lamps was set up and timed from a delay generator in a Tektronix oscilloscope (triggered initially by discharge of the laser flash lamp) to fire at the quarter and three-quarter periods of the pendulum. The peak to peak throw of the pendulum was measured from a photograph of the strobe illuminated scene via the traverse of a pointer (attached to the pendulum) relative to a fixed scale in the vacuum chamber. Figure II-3 shows the strobe photograph of the oscillation of the pendulum after the impact of the focused 13 joule 1.06 micron - 50 microsecond (5cm focal length lens) radiation onto a carbon pencil lead.

Figure II-4 shows integrated (or open shutter) photographs of the annular lamp-laser generated impacts onto vacuum mounted pyrolitic graphite and titanium samples. The lack of streamers are indicative of a low mass loss.

Inspection of the results summarized in Table II-1 show that the effective exhaust velocities were approximately a factor of 5 off of what was necessary or required to accelerate matter to meteor type velocities. In general, to continue one would require a laser of approximately four times the energy of the present annular lamp system, clearly beyond the capability of the present contract. The concentration on measurements with carbon targets was

TABLE II-2

Effective Exhaust Velocities Measured with the 50 Microsecond Neodymium Laser

Material	Sample Size	Laser Emission	Impulse via Vacuum Ballistic Pendulum Dyne-Sec.	Mass Loss Milligrams	Effective Exhaust Velocity C Kilometer/Second
Fe (dull rod)	0.060 inches dia.	∿13	43	0.6	0.7
Fe (dull rod)	0.060 inches dia.	∿13	42	0.4	1.0
C (9H pencil lead)	2mm	∿13	63	0.24	2.6
C (9H pencil lead)	2mm	∿13	64	0.23	2.8
"	"	"	57	0.23	2.5
"	"	"	66	0.28	2.4
"	"	"	60	0.28	2.2
"	"	"	58	0.22	2.6
C (Pyrolitic graphite)	1/4 x 1/4 x 3/8"	"	49	0.17	2.9
"	"	"	44	0.18	2.6
"	"	"	49	0.16	3.1
"	"	"	53	0.17	3.1
"	"	"	49	0.16	3.1

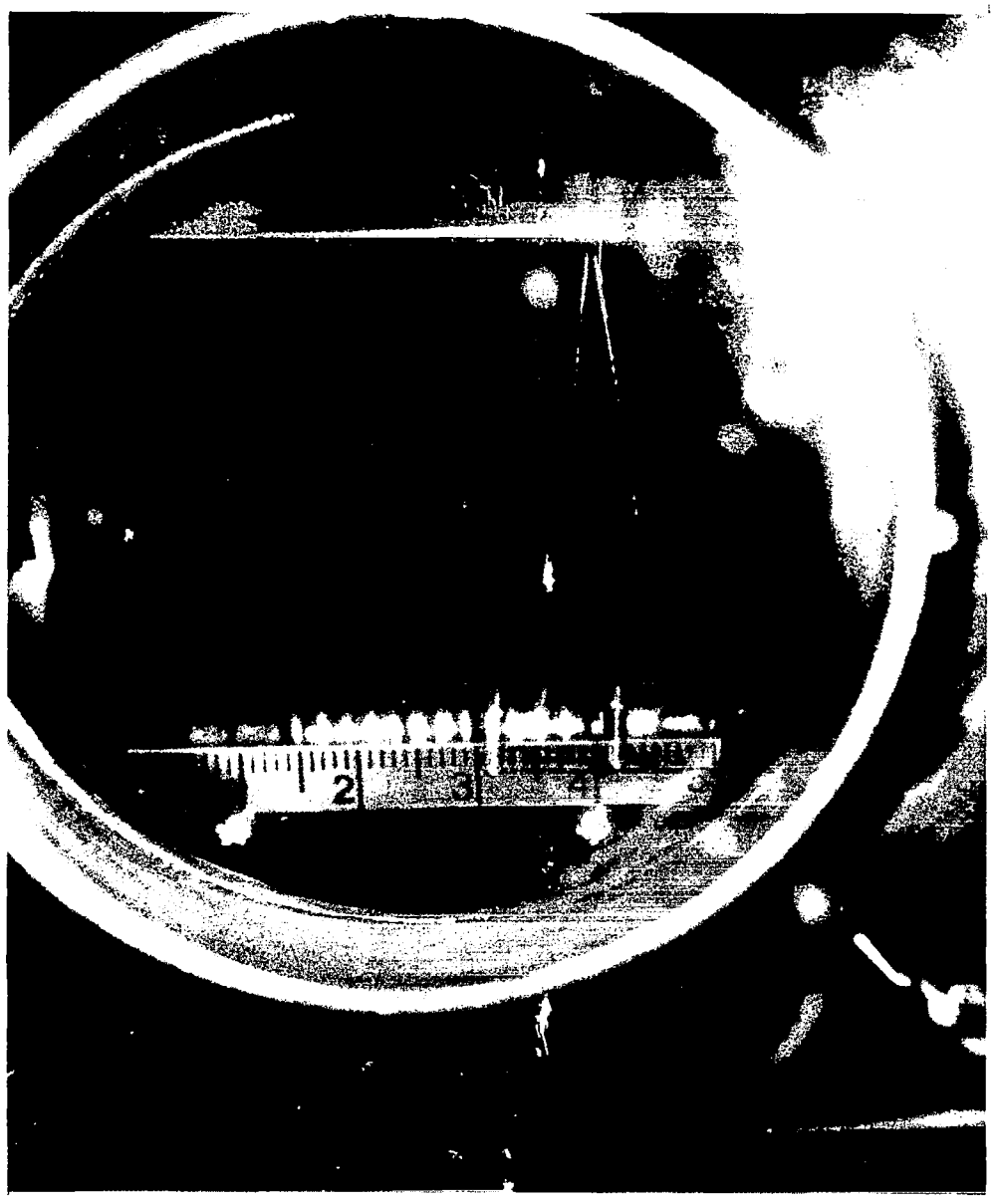

Figure II-3: "Double Strobe Light Photograph" of the vacuum mounted ballistic pendulum used to measure the impulse by focused laser radiation. Sensitivity of pendulum (in dyne-second) was 60 times peak to peak throw of pendulum. Thus, for the example shown (carbon), the impulse was 63 dyne-seconds ∿ and mass loss as measured before and after test was 0.24 milligrams (exit velocity, 2.7 kilometer/second). The sample was impacted by the radiation from a neodymium laser rod driven by the fast annular lamp. Two strobe lamps were set up to illuminate the chamber at the times of maximum plus and minimum displacements.

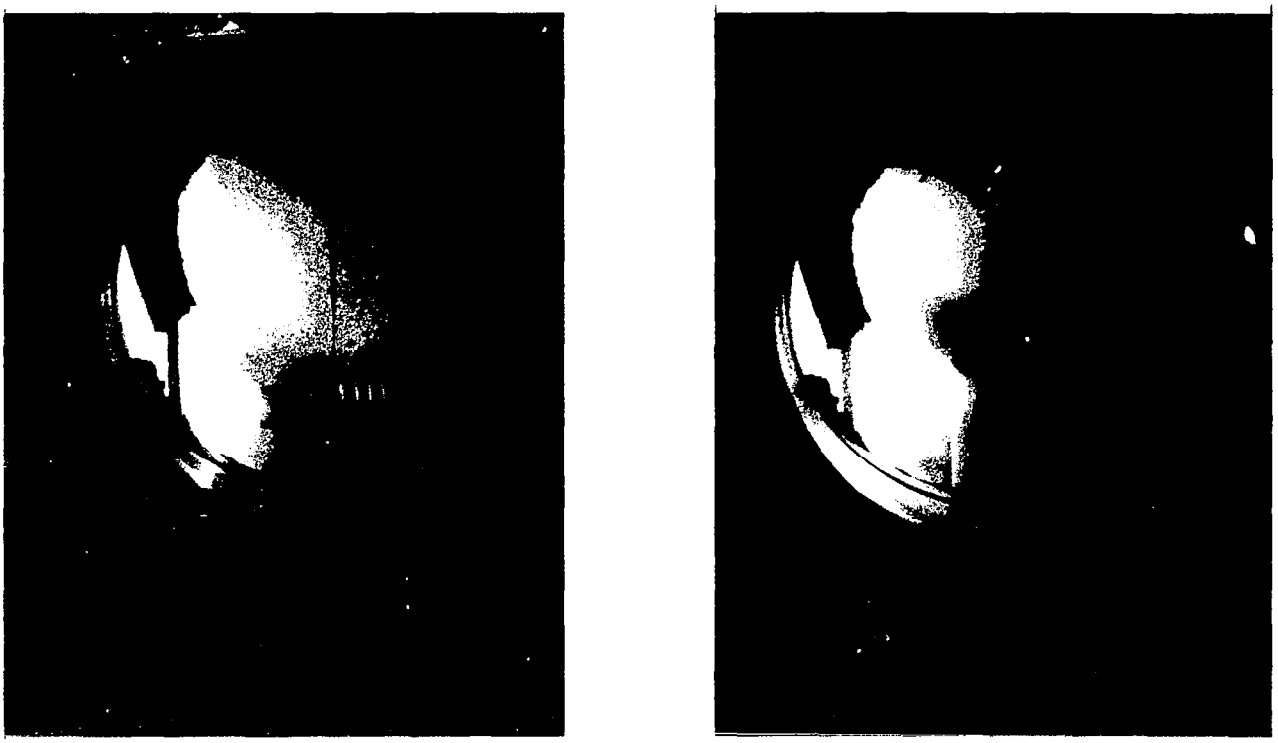

Figure II-4: Photographs of the laser induced vacuum ablation of pyrolic graphite (left photograph) and titanium metal (right photograph). Ablation was a result of focused radiation from the neodymium laser driven by the TRW annular flash lamp (∿50 microsec. duration.Lack of sparks or "streamers" is indicative of low mass loss and "high"effective exhaust velocity. Photograph was taken on 3,000 speed Polaroid film at f/32 and N.D. 2 before a lens.

a result of our understanding at that point that of all the materials so tested, carbon had been found to yield the highest exhaust velocities.

At this point it was decided that rather than continuing with the annular lamp system (at possibly slightly higher energies where the lamp was on the verge of explosion), that, rather, it was important to make measurements with a giant pulse laser system so as to at least know what sort of effective exhaust velocities would be achieved with laser systems of limiting flux densities.* The argument was that highest exhaust velocities should be produced by the focused radiation from a giant pulse laser, and that if these values were not sufficient, then a lack of feasibility had at least been established.

A Q-switch laser system with one stage of pre-amplification was assembled from laboratory supplies. The system is described in detail in Appendix II of this report. For the present discussion it is sufficient to state that this system emitted a 2.8 joules pulse of 0.694 micron radiation in approximately 100 nanoseconds.** The output was sufficiently collimated such that when focused in air with lenses of 9 centimeter or less focal length, "air breakdown" would be achieved. This phenomena was subsequently used to verify that the system was aligned and none of the components were dirty or had failed.

---

*The giant pulse solid state laser takes energy stored in the laser material (via optical pumping) and converts it into radiation in times of an order of magnitude of the light transit time between the end reflectors. As a result, they produce "ultimate" radiant power densities.

**The 100 nanosecond duration was the result of the large 1.5 meter mirror separation. The long cavity was found to give highest coherence and also lowest attrition on the optical components, particularly the Kerr cell and polarizing prism. Over the duration of this program no components were lost.

With the Q-switch ruby oscillator - amplifier system operating at maximum emission, impulses of 2 dyne-second were realized when either 9H pencil lead or pyrolitic graphite was mounted in the vacuum ballistic pendulum. Titanium wire samples gave impulses of 1.5 dyne-seconds. The craters were so small that the mass loss could only be estimated to be in the microgram range. Impulses with the giant pulse laser system were typically one-sixth that of the values realized with the intermediate pulse laser (see Table II-2) indicating that the fficiency for the conversion of optical radiation into ablation products is lower at multimegawatt power levels than at the hundred kilowatt range.

The preliminary impulse experiments with the giant pulse laser pointed up the need for mass measurements at the microgram level. The most accurate balance in the company and available to the program had a sensitivity of approximately 20 microgram.

In order to arrive at an early estimate of the effective exhaust velocity with the multimegawatt emission from the giant pulse laser, a number of experiments were conducted on samples onto which a large number of shots could be placed. For these experiments a new (0.686 gm) pendulum bob was constructed which would support half-inch by half-inch plates (typically 0.40 gms). The pendulum had a period of 0.43 seconds and according to Equation 1 a sensitivity of 0.82 dyne seconds per millimeter of peak to peak stroke. Plates (0.025 inch thick) of titanium were prepared, since the earlier tests had given indication that carbon was being crumbled by the Q-switch laser induced impulse. Two titanium plates were used as checks on the operator of the microbalance. All three were weighed and then after the test series all three were returned and reweighed. The results for a run of 35 radiation impacts is shown below in Table II-3

TABLE II-3 ABLATION OF TITANIUM PLATE BY 35 IMPACTS OF THE RADIATION FROM A 3 JOULE - 100 nsec Q-SWITCHED RUBY LASER

Sample	Before	After	
A	0.412900 gms	0.412874 gms	-26 ugms (control)
B	0.397417 gms	0.397388 gms	-29 ugms (control)
C	0.411327 gms	0.410957 gms	-370 ugms (test)

Sample A was never removed from the box in which the samples (after cleaning) were stored and transported to the chemical laboratory for weighing. Sample B was removed from the box and placed in the vacuum chamber but was not hit with the focused beam from the laser. The intent was to duplicate as close as possible the mechanical treatment given to the irradiated sample (i.e., C). For the sequence, the average mass loss per impact was 11 $\pm$ 1 microgram.

Throughout the test series the impulse for each shot was recorded by photographing the peak to peak stroke of the ballistic pendulum (sample shown in Figure II-5, along with the emission from the Q-switch ruby laser via an integrating biplanar photodiode. Suffice it to say that throughout the test series there was a variation of $\pm$ 10% in the measured impulse versus a variation of 5% in the shot to shot emission of the Q switch ruby laser system. The effective impulse per shot was 2.5 dyne seconds which when divided by the average mass loss of 7-10 micrograms gave an effective exhaust velocity of 2.5 kilometers per second. The value was not particularly encouraging from the point of view of feasibility of acceleration; however, it was noted that the material did not cleanly evaporate but evidenced some ablation in the form of particulate matter (see Figure II-5). Inspection of the titanium plate showed that the individual impact sites varied in size from one another and as a result could have had large variation in the ablated mass.

The sequence described above was repeated with a second set of samples and for a run of 100 individually monitored (i.e., impulse and integrated emission) Q-switched laser impacts. The initial and final weighing of the three samples are shown below in Table II-4; also, microphotographs of the plate are shown in Figure II-6. As can be seen, the average mass loss for the sequence was 5.5 micrograms. The impulse for the sequence was essentially the same as in the earlier thirty-five shot sequence ($\sim$2.6 dyne sec.), with the result that the effective exhaust velocity was approximately 5 kilometer per second or better than a factor of two greater than the previously derived value!

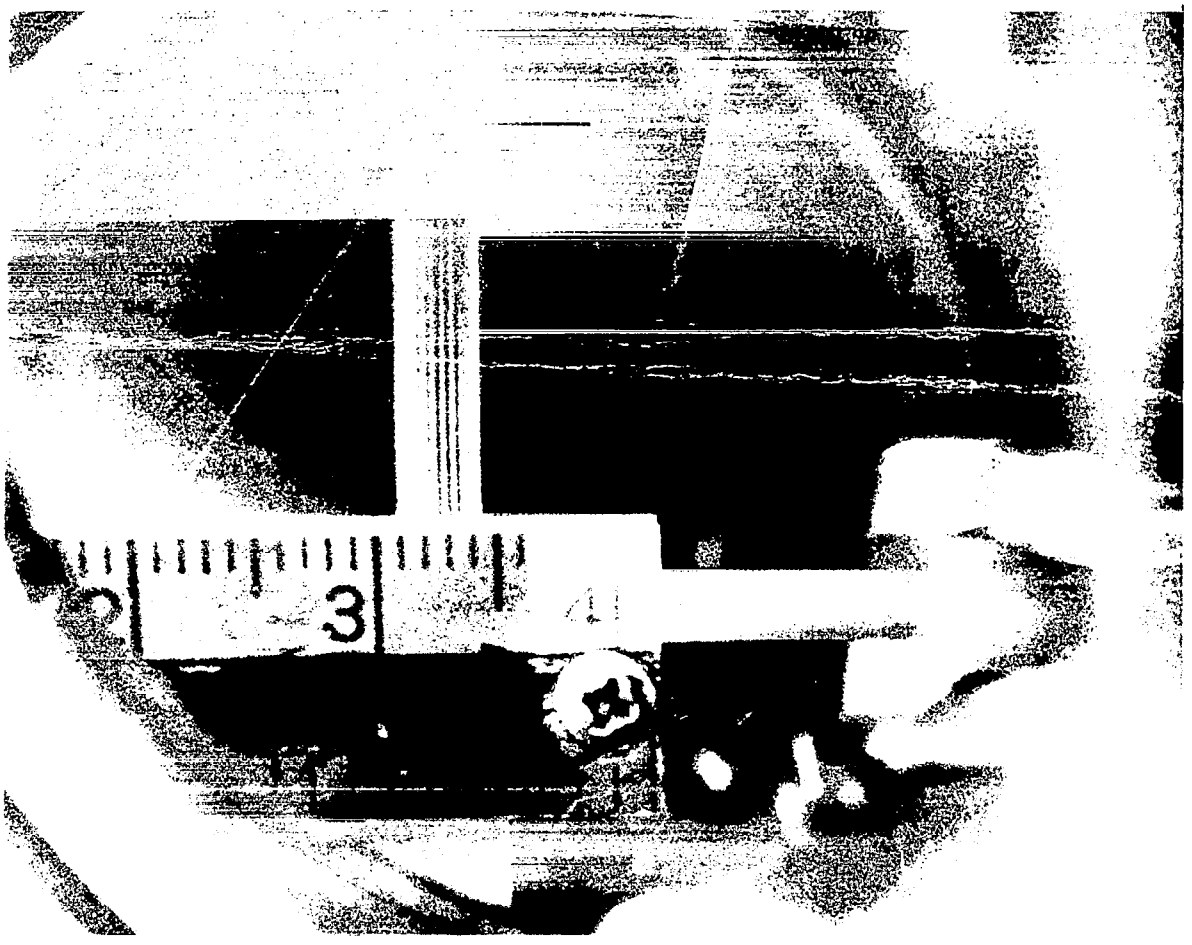

Figure II-5 Sample photograph of the oscillation of the evacuated ballistic pendulum (0.82 dyne sec/mm pk-pk) due to ablation of titanium by the focused radiation from a 3 joule - 100 nanosecond Q-switched ruby oscillator-amplifier system. The streaks in the photograph are the result of superheated particles.

TABLE II-4 ABLATION OF TITANIUM PLATE BY 100 IMPACTS OF THE FOCUSED RADIATION FROM A 3 JOULE - 100 nsec Q-SWITCHED RUBY LASER

Sample	Before	After	Loss
A	0.337810 gms	0.337815 gms	+5 μgms
B	0.465374 gms	0.464809 gms	-565 μgms
C	0.468662 gms	0.468663 gms	+1 μgms

The two runs indicated that there was a strong systematic error in the experimental technique which was associated primarily with the weighing technique. This was important due to the fact that the approximate factor of two discrepancy between the two sequences are borderline between feasibility and lack of feasibility.

In order to check the sensitivity of the impulse as a function of location of the ablating surface relative to the focal point of the concentrating lens, a series of measurements were made of impulses as a function of location off focus. The results are summarized by the graph shown in Figure II-7 and as can be seen, close to the focal point the impulse is essentially independent of the focal position. With increasing distance, the impulse increases, collaborating the higher impulse measurements per radiant energy as seen with the intermediate duration laser.

Also tested was the impulse as a function of intensity of the radiation from the Q-switched ruby laser system. Crude plots verified that the radiation was proportional to the energy of the laser pulse.

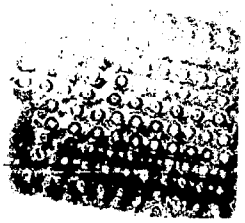

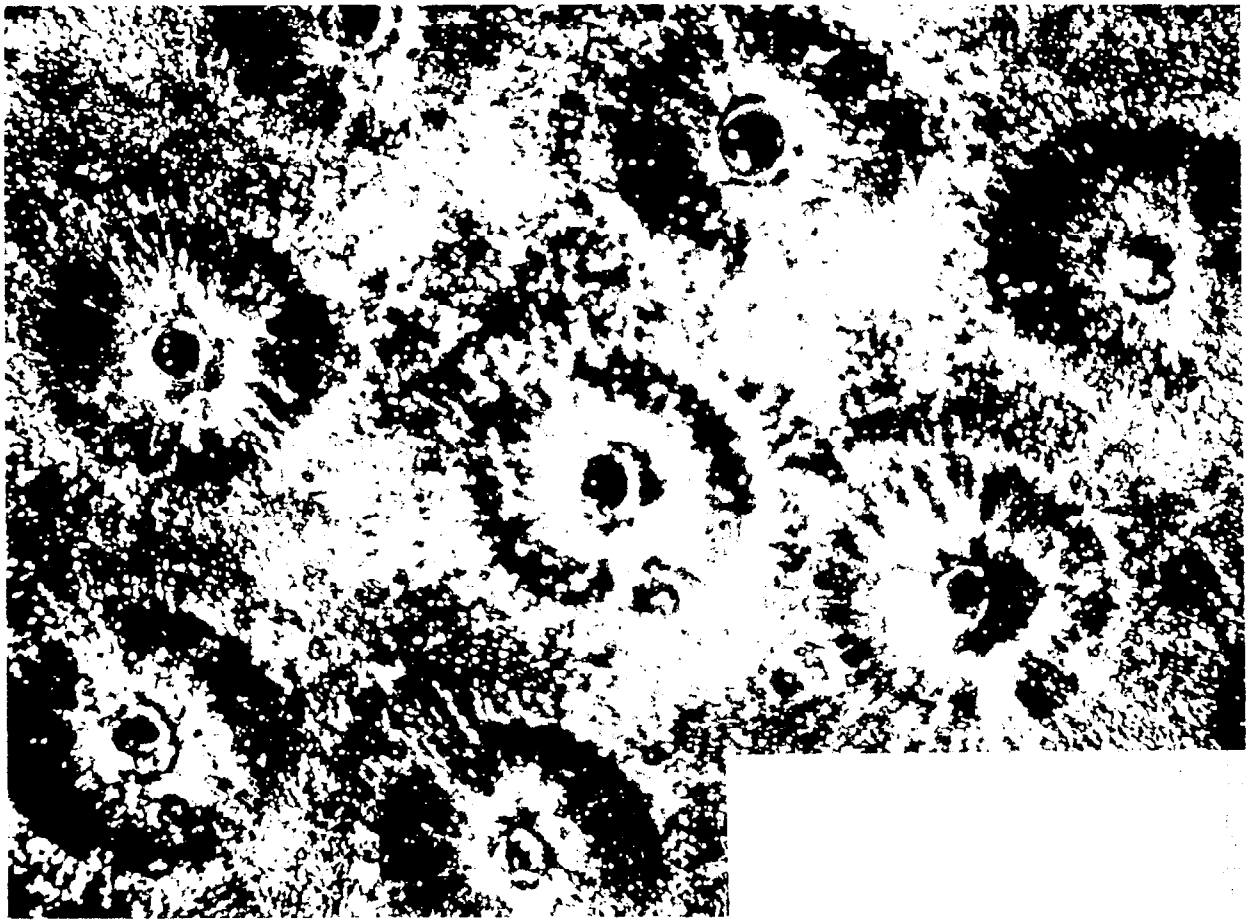

Figure II-6: Photographs of the 0.5 x 0.5 x 0.025 inch titanium plate after 100 pinpoints by the focused radiation from the 3 joule-100 nanosecond, Q-switched ruby laser. Upper photograph x 1.5. Lower photograph x 30, with photograph of 0.1 mm per division stage micrometer.

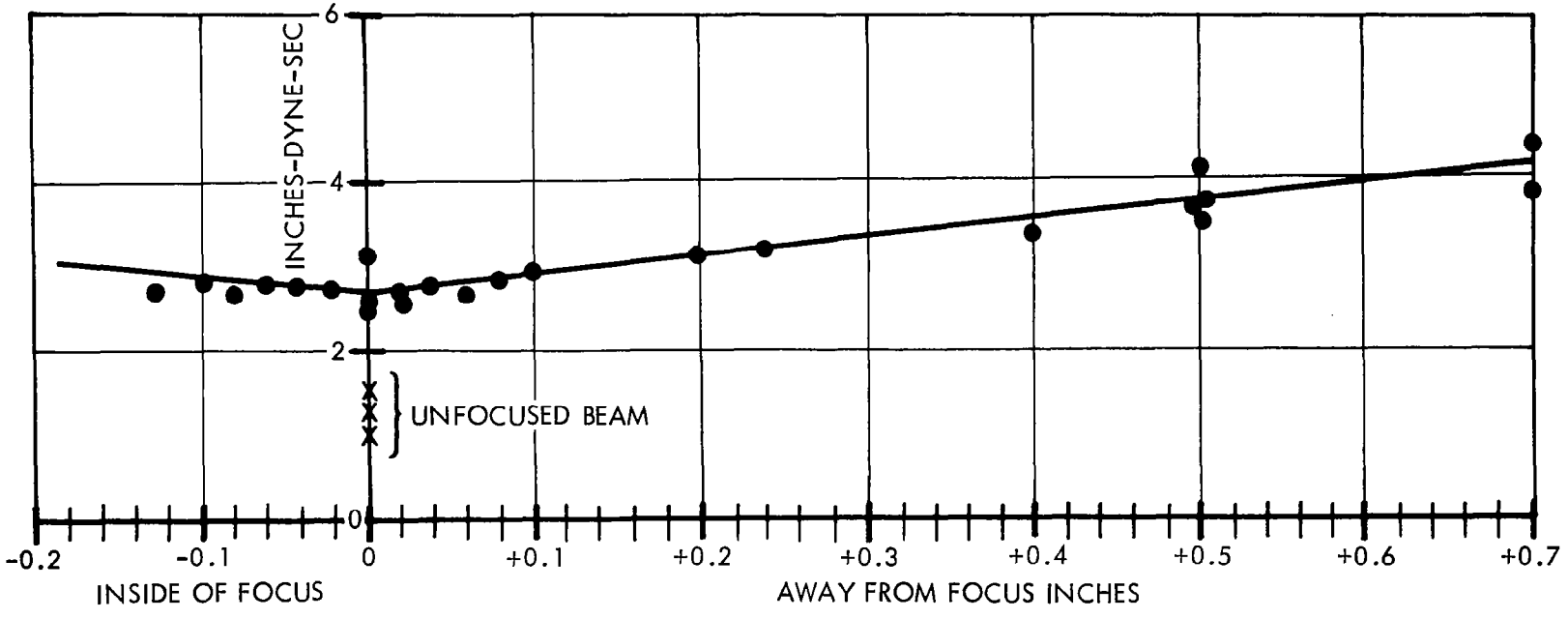

Figure II-7 Impulse delivered to a titanium plate (in the vacuum ballistic pendulum) by the 3 joule - 100 nanosecond radiant pulse from Q-switched ruby laser as a function of distance from the focal point of the 5 centimeter concentrating lens.

Other measurements were made but these were about as conclusive as the results cited above. Of interest were experiments with fine titanium wires (typically 0.015 inch diameter) which when hit with the focused light from the Q-switched laser system were bent. The result at least indicated that the energy densities were of the order of the yield strength of the material.

The measurements, if nothing else, demonstrated the weakness of the program in so far as our ability to measure the ablative mass loss. Recognizing the need to achieve accurate mass measurement, effort was deliberately spent on the development and perfection of a technique with sufficient sensitivity to deduce effective exhaust velocities on an individual shot to shot basis with no further increase in the size of the laser apparatus.

In addition to setting the stage for the program, the measurements indicated that the laser systems were operational and that materials had been found (chiefly titanium) which at least gave effective exhaust velocities approaching the values of interest to hypervelocity acceleration of matter. As noted above, a factor of 2 in the measurement of either the impulse or ablated mass was the difference between feasibility and lack of feasibility.

CHAPTER III

DEVELOPMENT OF THE REED MICROGRAM MASS MEASUREMENT TECHNIQUE

The determination of the effective exhaust velocity of matter evaporated or ablated by the focused energy from a pulsed solid state laser required mass loss measurement to submicrogram gram accuracies. A search of the literature on ultimicrobalances showed that although quartz fiber ultramicrobalances of the proper sensitivity had been developed, these instruments were susceptible to vibration and air currents.*+ For measurements in the microgram range, the measurement times were in addition too long (∿several hours?).

Further, for the present problem we were interested not in absolute mass determination, but rather the amount of mass lost via ablation (i.e., differential measurements). In addition, a device which would combine both impulse and mass loss measurement would be ideal, and the quest for such an apparatus turned us away from any further consideration of either the conventional quartz fiber or taut wire magnetic microbalances.

A mechanical, electrically sustained, vibrating reed was proposed as the means of making mass measurements to the required degree of accuracy as well as simultaneously measuring the impulse. Mass loss would be related to the change in the resonant frequency of the reed while the impulse would be related linearly to the initial amplitude to which the undriven reed was set by the impact of the laser beam.

The first reed oscillator was built from a 0.07 x 0.01 inch (cross-section) by a 7 millimeter long jeweler's saw blade. The reed was clamped at one end and driven in the three quarter wavelength mode by magnetic coils at the nodes (one being a pick-off, the other being a driver) of the vibrating bar. The coils were interconnected by an oscilloscope preamplifier of Gain 500. The period of the reed was measured with a Beckman 6146 Counter and was initially 1,668 milliseconds. Calibration of the reed

---

*Encyclopedia Britannica, Volume 2, Annual Register to Baltic Sea, Encyclopedia Britannica, Inc., William Benton, Publisher, Chicago, London, Toronto, 1960 (p. 951).

+A Cahn servo-balanced microbalance is owned by another group in TRW Systems. Although the unit was claimed to have sensitivity in the tenth microgram range, conversations with the TRW personnel who operate the balance indicated that such sensitivity was difficult, if not from a practical standpoint, impossible to achieve. The balance was used only to sense evaporated loss in a vacuum chamber to 10 micrograms.

oscillator was achieved by accurately cutting a small piece of wire (150 microgram) from a larger (1 meter long) weighed piece and measuring the periods before, with the added mass, and after removing the mass (1.6641, 1.6947, and 1.6648 milliseconds, respectively). The calibrated sensitivity was found to be 5 micrograms per microsecond. This first vibrator did not have a stable steady frequency but rather drifted at a rate of 0.4 μgm per second. The drift was due to the highly temperature sensitive elastic constant of the steel reed. In spite of the above difficulties, the reed was set up (in air) at the focal spot of the laser and hit with the radiation from the Q-switch laser source. The following changes in mass were deduced from the change in the period of the reed: namely, 4.5 micrograms; -1.5 micrograms; 8 micrograms, no change; 5 micrograms; and 10 micrograms. Operation of the reed in air lead to a strong air breakdown which might have accounted for the unexpected measurements of changes in mass of the reed; however, the thermal sensitivity was the more logical choice.

This first reed oscillator was, in fact, not sensitive enough to mass changes and was sensitive to thermal changes. The exercise did demonstrate that a reed oscillator could be built with a modicum of equipment and that such an oscillator would be capable of sensing microgram and submicrogram mass changes. The reed could not simultaneously measure impulse due to the fact that it struck one of the drive coils when hit by the laser.

The next step in our quest to submicrogram differential mass measurement was the procurement of the movement from an Accuratron watch. This time piece is based on a highly engineered tuning fork oscillator with fixed pole tips at the ends. The period measured with the Beckman Counter was 2,777.7640 $\pm$ 0.0005 microsecond and the mass calibration was 470 micrograms per microsecond (considerably less than the reed vibrator previously described). Small copper sheets were glued (Ducoa cement) to the ends of the tuning fork and to these were attached the test samples. For first tests a piece of 9H pencil carbon was glued onto the vertical veins.

The impulse sensitivity of the Accuratron tuning fork vibration was determined by dropping a steel ball bearing of known mass from a known height and measuring (via an oscilloscope) the voltage induced in one of the pickoff coils. The sensitivity was found to be 3.3 dyneseconds per peak to peak volt.

The system was mounted in the vacuum chamber with the center of the carbon sample at the focus of the concentrating lens. The period of the fork was monitored with the Beckman counter for about thirty separate determinations. The battery powering the transistor was opened and the laser beam fired into the carbon sample. An oscillogram of the induced voltage on the coil was recorded. After the shot, the battery was reconnected and the period of the clock monitored for another twenty or more separate determinations. The measured periods were then plotted against time. The change in period at the time of impact was determined by extrapolation of the plotted curves. For one determination, the period changed by 0.03 microsecond or 14 micrograms. The impulse was 1.2 volts peak to peak or 3.8 dyneseconds. The effective exhaust velocity was accordingly 2.7 kilometers per second.

Compared to the first reed oscillator the Accuratron movement had proper impulse sensitivity but was an order of magnitude too insensitive to mass change.

Another separated measurement with the added carbon simply gave an impulse of 1.5 dynesecond, a mass loss of 3 micrograms, corresponding to an effective exhaust velocity of 4.6 kilometers per second. Other measurements gave an impulse of 1.3 dyneseconds with a mass loss of 7 micrograms, for an effective exhaust velocity of 1.9 kilometer per second; 1 dynesecond with a mass loss of 2.5 micrograms for 4 kilometer per second effective exhaust velocity; 1.4 dynesecond with 5 micrograms mass loss for 2.6 kilometer per second; 1.3 dyne second and 2.5 micrograms, respectively, for 5 kilometer per second effective exhaust velocity.

An inspection of the carbon target indicated that the hole sizes were not uniform and it was suspected that chunks were being torn loose

by the high mechanical stresses by the laser impacts. The results were encouraging at least to the extent that some measurements showed effective exhaust velocities of values approaching those of interest to the present program.

The Accuratron watch, although close, was just not sensitive enough. In addition, the measurements were subject to criticism on the score that the frequency of the oscillation of the fork was sensitive to the position of the added test sample. The bending or displacement of the sample could give erroneous mass changes.

Tests with a shorter focal length lens ($\sim$3 cm) gave a 2 microgram loss and a 1.2 dynesecond impulse for an effective exhaust velocity of 5.5 kilometers per second. When the Accuratron fork was operated at atmospheric pressure (in the presence of an air breakdown) mass loss was 18 micrograms with an impulse of 0.8 dyneseconds. Tests were also made in the regular lasing mode by removing the bias from the Kerr cell in the ruby laser oscillator. Regular lasing impacts were measured; for example, for 3.6 joules of laser radiation the impulse was 6.8 dyneseconds, the mass loss was 32 micrograms, and an effective exhaust velocity was 2.1 kilometers per second. For 3 joules of regular emission the impulse was 4.1 dyneseconds, the mass loss was 13 micrograms, and the effective exhaust velocity was 3.1 kilometers per second. The results were in close agreement with earlier regular lasing shots measured with ballistic pendulum and the Mettler balance.

The preliminary measurements summarized above lead finally to the development of a reed vibrator which could make mass measurements to an accuracy of 0.1 microgram. The vibrator was based upon an Elinvar reed having a natural frequency of 324 cycles per second. The description and operation of the final device is described in a separate section of this report.*

*Appendix I.

CHAPTER IV

THE FREE ACCELERATION OF SMALL PARTICLES

Up to this point in the program, all of the attempts to measure the effective exhaust velocities of matter ablated by pulsed laser radiation had been conducted with large millimeter sized samples either mounted in ballistic pendulums or attached to the end of one of the prototype reed oscillators. All of the measurements were weak in the sense that they were being made on samples which were large compared to the (100 micron) size range of interest to the present program and large compared to the focal spot size of the laser beam.

In order to begin to get some feel for the impulse and velocity which 100 micron sized particles could be accelerated by the radiation from a laser, a series of free acceleration experiments were begun. For these tests the ballistic pendulum was removed from the small three port vacuum chamber mounted upon the microscope micromanipulator. A lead zirconate piezoelectric crystal was attached onto the inside surface of one of the Plexiglas windows and connected via a wax vacuum seal to an external oscilloscope. The particles which were to be accelerated were imbedded in a submicron thick lacquer film which was supported on a metal frame with 1/4-inch perforations.* The particle bearing frame was placed before the opposite Plexiglas window at a known distance from the surface of the piezoelectric detector (typically 6.7 centimeters). While the chamber was being evacuated, the chamber was positioned with the drive units on the micromanipulator until the image of a particle was superimposed onto the cross hairs of the sighting telescope (coincident with the focus of the laser beam). The cross hairs of the telescope were observed, in turn, with a microscope having a calibrated travelling eyepiece, thereby making it possible to measure the diameter of the particle before it

*The particle bearing frames were prepared by a technique common in the preparation of films for electron microscopy; namely, clear lacquer was poured out upon a free water surface and while not dry, dusted with the test particles. Upon drying, the particle bearing film was then transferred to the metal screen by slipping it under the surface of the water and then withdrawing it with the lacquer film attached. The thickness of the film could be judged from interference colors when the perforated screen was held up to an incandescent lamp.

was struck by the laser beam.* For spherical particles, the initial mass could be calculated from the measured diameter and initial density.

After a particle had been both located at the focus of the laser source and measured, it was then launched by the 3 joule - 100 nanosecond radiant pulse from the ruby laser oscillator - amplifier system. The laser pulse was monitored by a biplanar photodiode which, in turn, triggered an oscilloscope monitoring the piezoelectric crystal. The transit time of the laser accelerated fragment (between the support frame and the piezoelectric crystal) was measured from the recorded oscillogram and the velocity calculated from the known separation.

In addition to measuring the velocity as a function of the estimated initial particle size, the detection technique made it possible to note whether a particle arrived as a single fragment or whether it was broken up into a multiplicity of fragments by the laser impact. Particles which fragmented repeatedly were indicative of laser forces of acceleration in excess of the yield strength of the material. For example, diamond dust (obtained from lapidary paste) and titanium carbide granules were found to shatter when struck by the focused beam from the laser oscillator-amplifier system.

Figure IV-1 shows a Polaroid photograph of the apparatus at the time it was being used to measure and to freely accelerate the different microparticle samples. The photograph has been cut to remove extraneous background and to identify some of the component parts. The focusing lens was mounted at the end of the rail in a separate holder with a Plexiglas support. Next came the aiming telescope and measuring micrometer which were attached to a separate housing and in which was placed a right angle prism+ (on an adjustable three-point carriage) oriented so that the axis of the telescope was coincident with the axis of the beam from the laser. The solid state laser

*The focusing and observing system was calibrated by placing a microscope stage micrometer at the focal plane and comparing the divisions of the stage micrometer with those of the travelling eyepiece.

+The right angle prism was removed after a particle had been sighted and just prior to firing of the laser. The prism had the feature of blocking the output of the laser in case of an accidental firing.

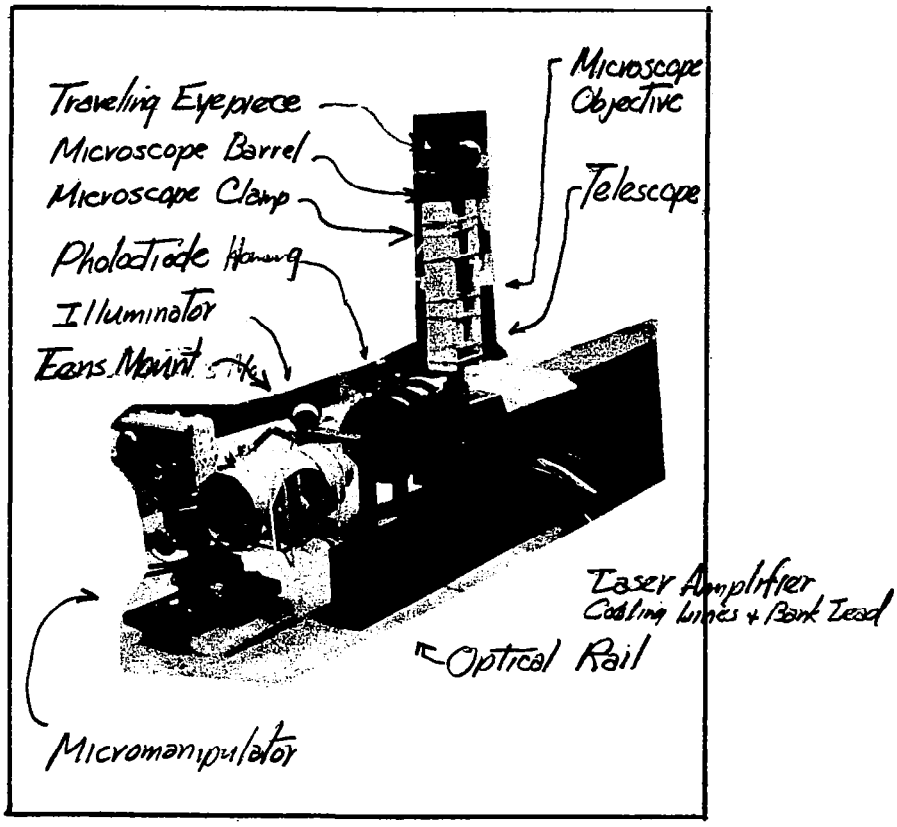

Figure IV-1. Photograph of the apparatus for the free acceleration in vacuum of ∿100 micron particles by the focused 3 joule ∿0.1 μsec beam from a Q-switched ruby laser oscillator - amplifier system. The particles were embedded in sub-micron lacquer film in the vacuum chamber on a microscope micromanipulator. The focusing, aiming, and particle size measuring optics, and the laser system were mounted on a common optical rail to the right of the vacuum chamber. Particle size (prior to acceleration) was measured with the calibrated eyepiece. A photodiode caught the light scattered from the focusing lens and triggered the oscilloscope which monitored the output of piezoelectric crystal (not shown) mounted onto the far window of the vacuum.

oscillator and amplifier* are attached to the same rail behind the alignment housing. The photodiode can be seen to the right of the optical rail along with the microscope illuminator which shines through the plastic focusing lens support, through the Plexiglas vacuum window, and onto the particles mounted within the lacquer film in the support plate. The rear vacuum window (on which the piezoelectric crystal was mounted) was left out of the photograph. The system as shown was straightforward in operation. About twenty separate shots could be taken before the perforated screen had to be replaced with a new one.

Figure IV-2 shows the results of the acceleration of titanium microspheres manufactured by the Linde Company. For this set of experiments the supporting screen and peizoelectric crystal were separated by 6.6 centimeters. The data is plotted in terms of the transit time (ordinate) of a laser accelerated fragment from the point of launch to the piezoelectric crystal detector versus the initial mass of the particle as computed from the measured diameter and the value of density found in the standard textbooks (4.5 gms/cm^3). Highest velocity was 3.3 kilometers per second for an initially 0.9 microgram particle. Particle fragmentation is noted by interconnecting the two piezoelectric sensed arrival times via lines. The experiment showed that particles of initial mass less than a microgram never arrived in large enough fragments to be detected by the pressure sensitive crystal, strongly suggesting as a result that these particles were completely vaporized by the laser beam. The fact that the experimental points fell upon an almost straight line was unexpected and gave us the false hope that the effective exhaust velocity might be deduced from the slope or intercepts of the experimental curve. In fact, it was the discovery of the above curve which lead us to recast the theory in the way that it was presented in Chapter I and attempt to draw some information from it. For example, as shown in the opening section a plot of the reciprocal of the final velocity versus the initial mass should have a slope equal to the product of the velocity and the amount of mass ablated. The curve shown in Figure IV-2 has a slope of 1 sec/cm gm. Assuming an

*See Appendix II.

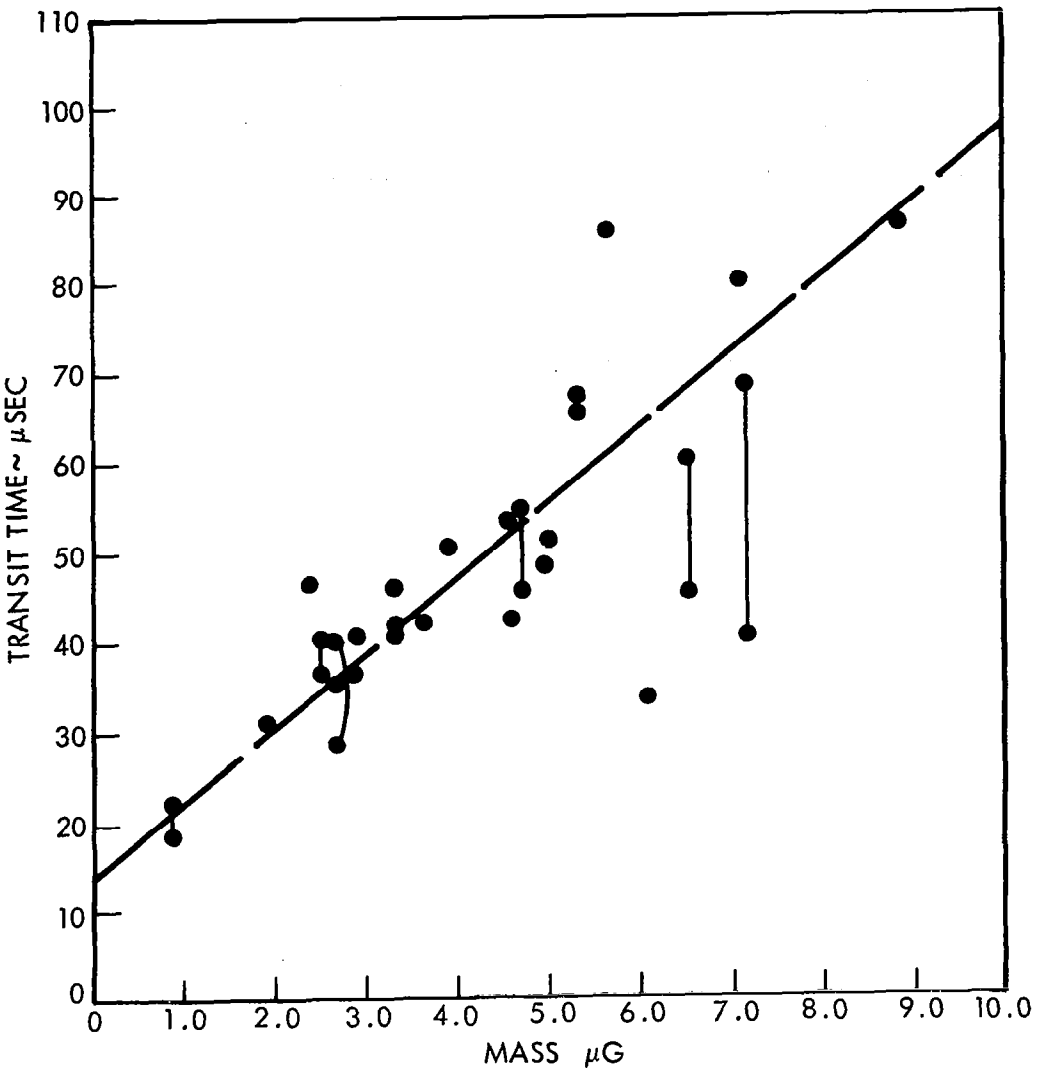

Figure IV-2. Acceleration of titanium spheres by the focused radiation from a 3 joule, 100 nanosecond ruby laser system. Flight path 6.6 cm, ordinate is the transit time in microseconds, abscissa. The initial mass measured with a microscope having a calibrated travelling eyepiece.

ablation of 1 microgram (since particles less than one μgm were not detected) one then arrives at an effective exhaust velocity of 10 kilometer per second for spherical particles of the size of interest to the present program.

At this time we were at a point where the feasibility of the program hinged upon the assumption of a one microgram mass loss! The fact that the curve did not intersect the positive initial mass axis could be accounted for by the fact that the initial particle size was less than the focal spot size of the laser. Theoretical models were constructed in an attempt to account for the departure but none of these were particularly satisfying and each lead to a different prediction to the amount of mass ablated.

Figure IV-3 shows the results when nickel microspheres were freely accelerated in vacuum. While Figure IV-4 shows what happens when tungsten microspheres are accelerated by the giant pulse oscillator amplifier system. The decreasing terminal velocity with higher atomic number materials is all that is intended to be indicated by the two attached curves.

Other spherical materials (such as chilled iron shot, aluminum, and magnesium) were ordered, but did not arrive until after funds for the program had been expended.

The free acceleration tests at least demonstrated that some rather impressive velocities could be achieved by "blitzing" in a vacuum titanium spheres with the focused radiation from a Giant Pulse Laser Oscillator - Amplifier System. The results also gave some glimmer of hope that the effective exhaust velocities at least for titanium may in fact be sufficient to accelerate this material to meteoric or near meteoric velocities.

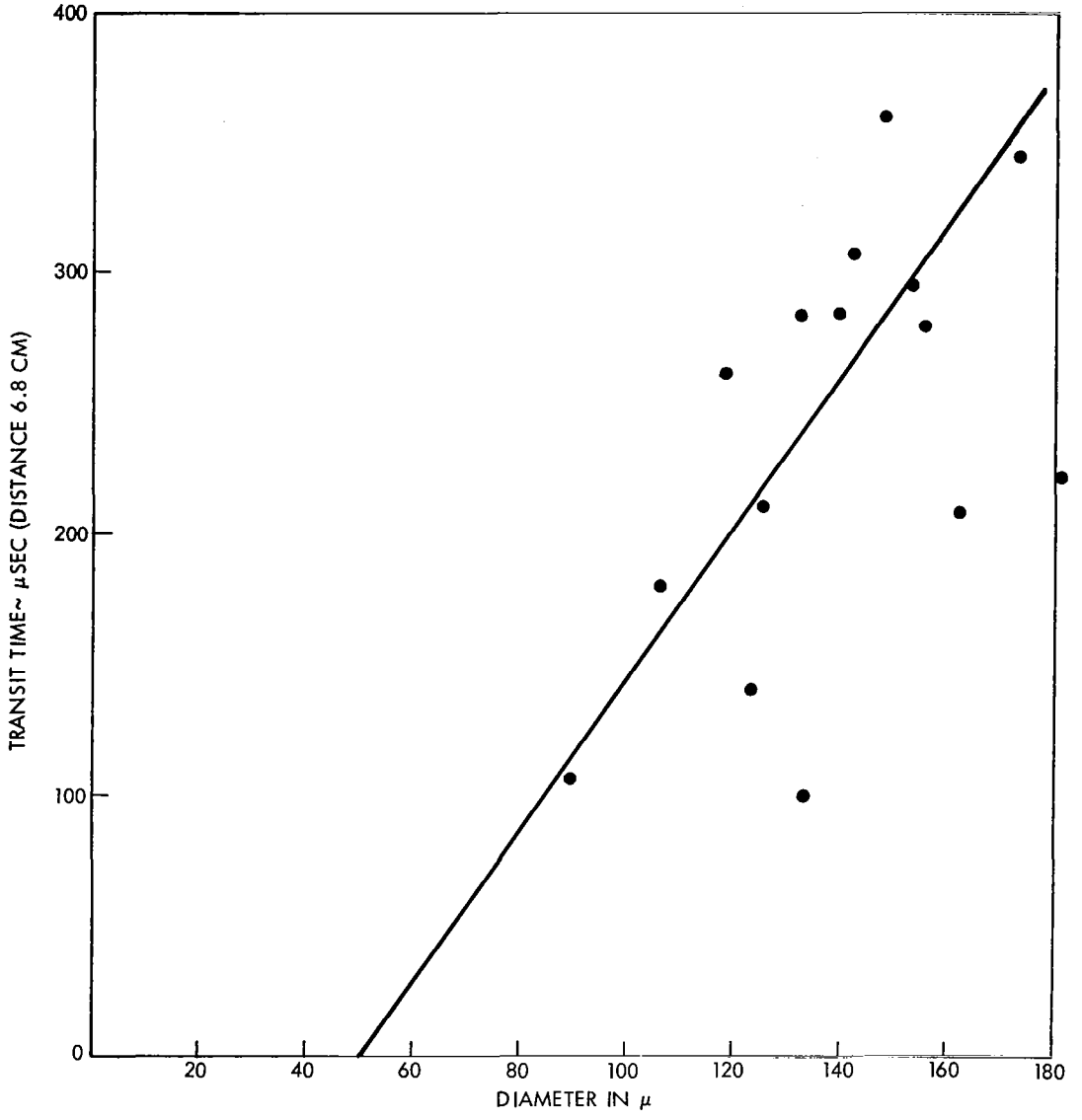

Figure IV-3. Acceleration of nickel microspheres by the output of a 3 joule, 100 nanosecond giant pulse Q-switched ruby laser. Flight path 6.8 cm, ordinate is transit time in microseconds; absicissa is initial particle diameter measured with the calibrated aiming telescope.

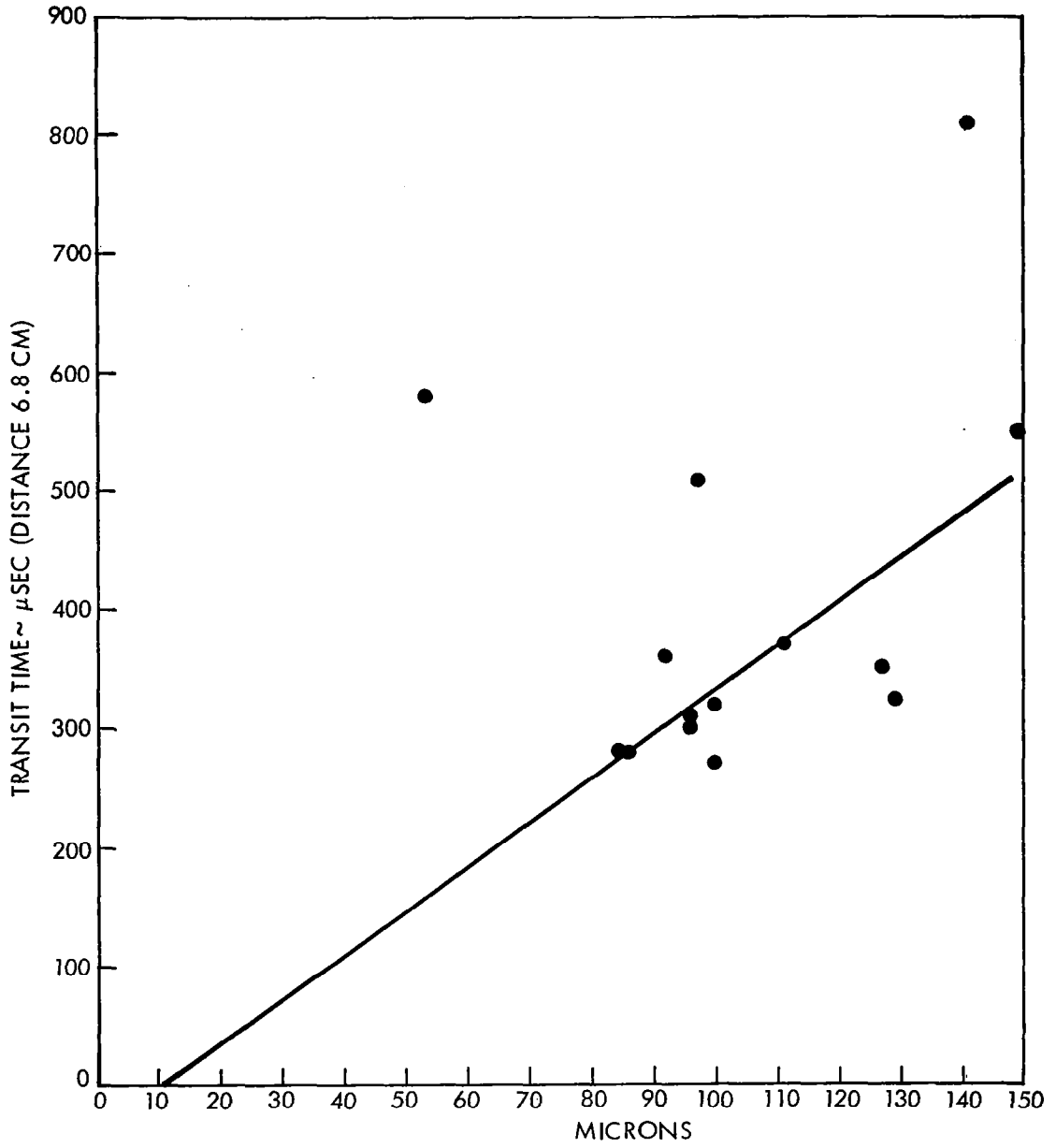

Figure IV-4. Acceleration of tungsten microspheres by the output of a 3 joule, 100 nanosecond Q-switched ruby laser. Flight path, 6.8 cm in length; ordinate is transit time of path in microseconds; abscissa is the diameter in microns.

CHAPTER V

MEASUREMENT OF THE EFFECTIVE EXHAUST VELOCITIES

The measurements on the free acceleration of metallic microspheres and other particles, as described in the previous section, demonstrated once again that the measurement of the effective exhaust velocity required knowledge of the amount of mass ablated by the focused laser beam.* In addition, we knew that titanium metal particles could be accelerated to rather formidable velocities. We were also convinced that measurements on larger millimeter sized samples were academic due to the uncertainties in scaling the effective exhaust velocities down to the particle sizes of the order of the focal spot size of the laser.

Earlier tests (described in Chapter III) with the Accuratron watch movement and with the prototype reed vibrators gave encouragement that the electrically driven approach could, in fact, lead to a weighing technique of sufficient accuracy.

Thus, to make measurements of the effective exhaust velocity we needed only to perfect a weighing machine and perfect means for recovering each fragment after it had been accelerated. Tests were conducted which lead to our discovery that fragments could in fact be recovered from paraffin, that the piezoelectric crystals could be coated with paraffin, and that paraffin coatings typically 3-4 millimeters thick did not adversely affect the sensitivity of the piezoelectric detectors.

---

*Much consideration was given to the use of a ballistic pendulum to measure the momentum of an accelerated fragment. The final mass of the fragment was to be deduced by dividing the impulse by the velocity as measured by the transit time technique. This approach required the development of a ballistic pendulum with a piezo electric bob, and was subsequently abandoned due to the low confidence in our ability to build pendulums of high enough accuracy. Another weakness was the large systematic error possible in the measurement of initial particle mass via a calibrated microscope due to the fact that a 10% error in measurement of particle diameter leads to a 30% error in the measurement of the mass.

A photograph of one of the paraffin coated detectors is shown in Figure V-1; the black specks seen in the picture are particles fragments accelerated by the laser. Figure V-2 shows the "single hole" mounting plate (in the end of the vacuum chamber) with a lacquer film onto which single particles were placed prior to acceleration with the laser. The surface of the aluminum frame is marked by the three aiming shots.

Thus, the program was dependent on the development of a microgram measuring device with truly microgram sensitivity. Thanks to the well equipped home workshop of Dr. L. O. Heflinger and some of his homemade high gain audio amplifiers, the procurement of a sample of Elinvar from the Hamilton Watch Company, and some piezoelectric crystals made by C. Knox (in his home shop), a particle weighing device was constructed which proved to have both the stability and sensitivity to make measurements in the microgram mass range. The completed device is described in detail in the Appendix I of the report.

Particles were prepared, weighed with the reed vibrator, transferred to a lacquer film, placed in the vacuum chamber at a measured distance from the paraffin coated piezoelectric sensor, evacuated, located at the focal plane of the laser, measured via the calibrated eyepiece, accelerated (by the radiation from the laser) into the paraffin cap on the piezoelectric crystal, recovered, washed in 1, 2, 4-trichlorobenzene (to remove excess paraffin), and finally reweighed. The velocity of the fragment was calculated from the oscillogram of the transit time.

The results of 25 separate measurements are presented on Table V-1. The first column of this table gives the code number of the particle, wherein the abbreviation WP stands for "weighed particle." The next column gives the material, then the focal length of the lens, the initial shape of the particle,* the initial diameter, the initial mass

*Cylindrical particles were cut from etched wires with a sharpened Exacto knife. This form was chosen over sphere since it was expected that the coupling of the plume would be better for cylinders versus spherical particles. As a result, it was expected that the effective exhaust velocity would be greater. The experiments bore this fact out. (Compare in particular WP #6 with the other measurements). Particles 3, 4, 8, and 10 were cut from normally 0.012 inch titanium wire; particle #5 was cut from titanium wire etched down to nominally 0.004 inches.

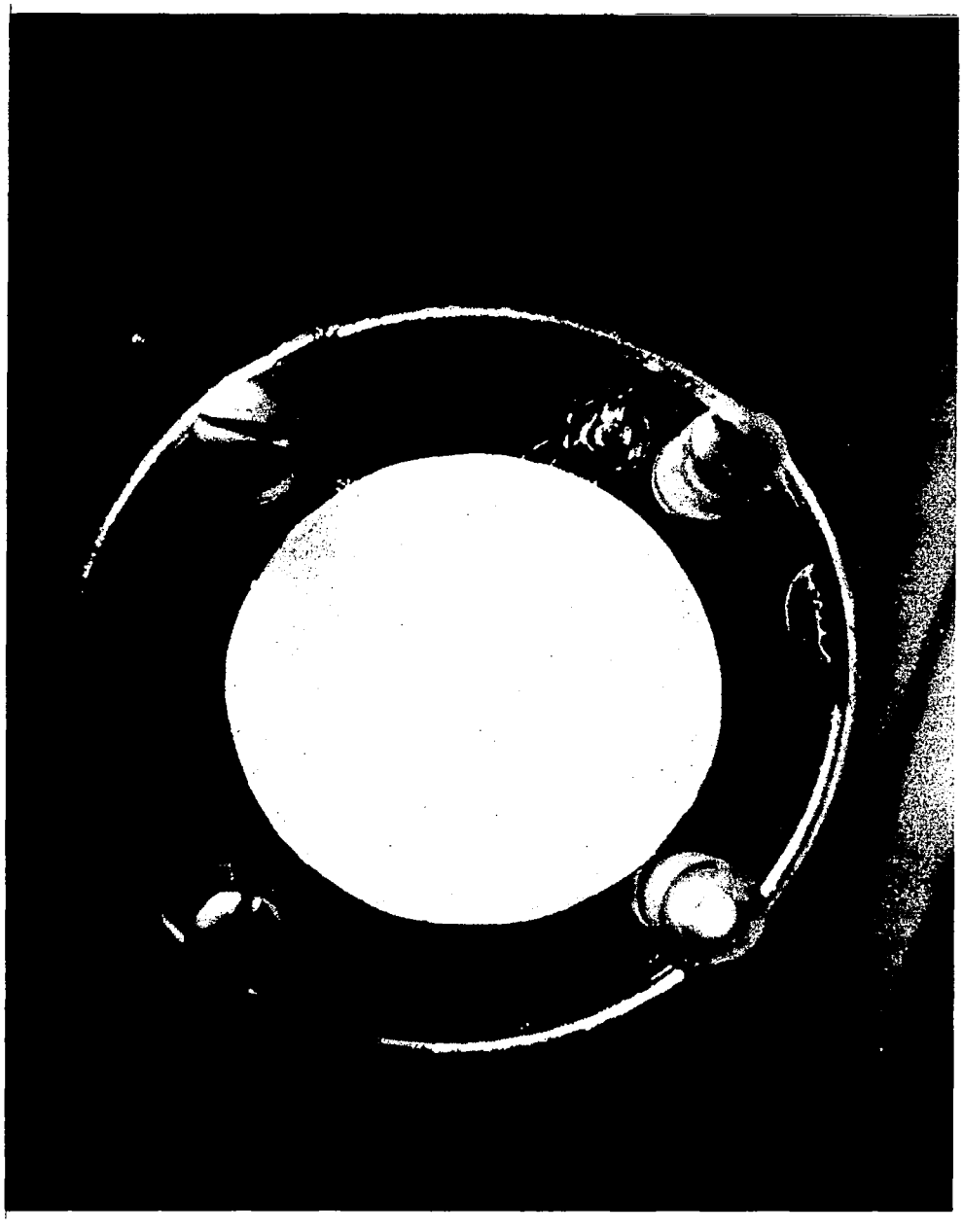

Figure V-1: Photograph of the end of one of the paraffin capped piezoelectric particle detectors as mounted onto one of the Plexiglas windows and with one of the micro-co-axial plugs. The four standoffs were used to support (in early days) an opaque membrane over the face of the detector. Careful scrutiny will show two impacted fragments in the surface of the detector.

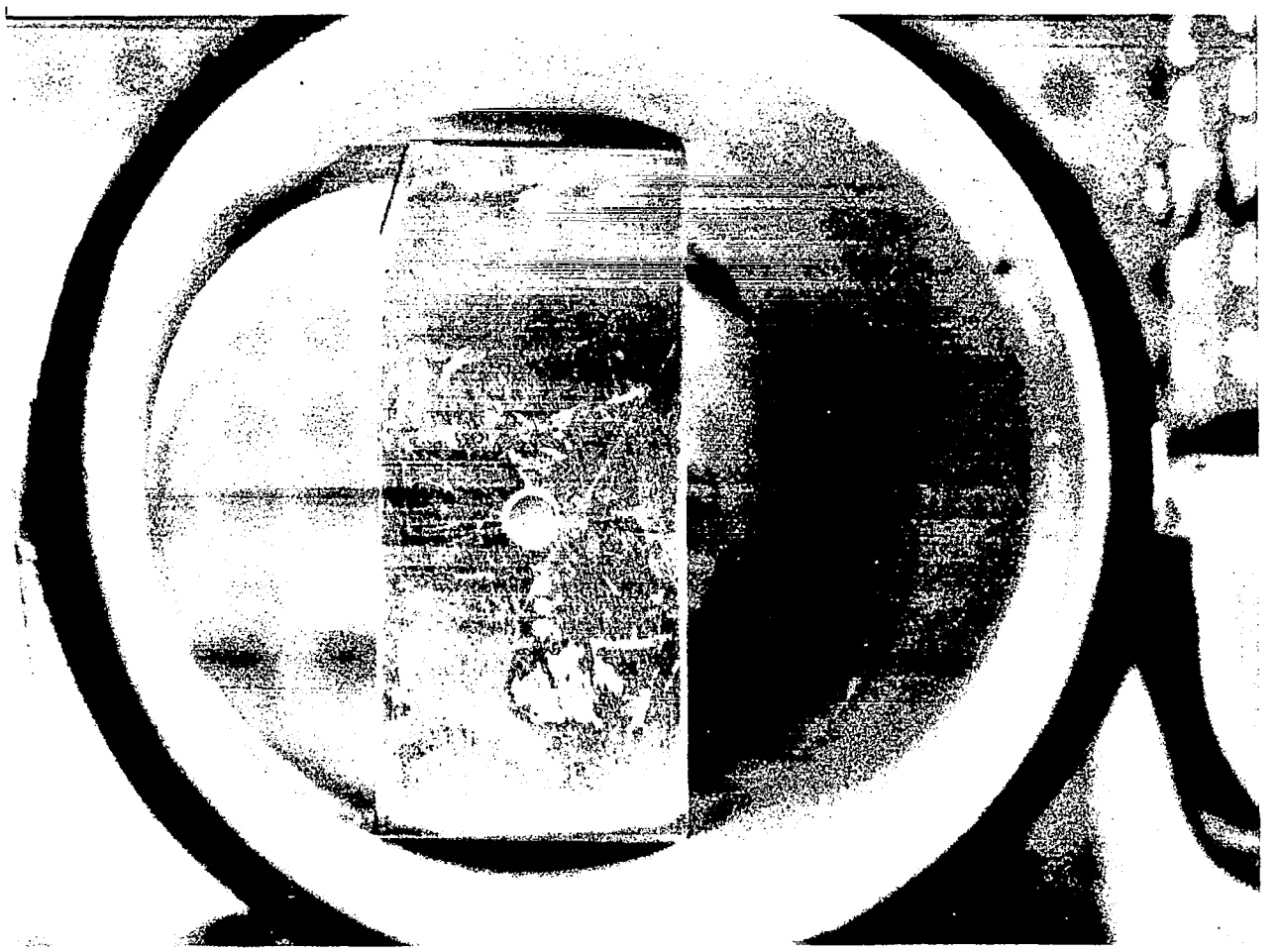

Figure V-2: Photograph of the end of the vacuum chamber with one of the single aperture mounting plates in place. The lacquer film was placed over the hole and the particle to be accelerated placed onto the film over the hole.

TABLE V-1 (Continued)

Q-SWITCHED (3 JOULE - 100 NANOSECOND) LASER INDUCED EFFECTIVE EXHAUST VELOCITIES

VIA ACCELERATION OF FREE PARTICLES (CONTINUED)

Code	Material	Lens focal length cm	Initial Shape	Initial Diameter microns	Initial Mass M_o µgms	Final Mass M_f µgms	Mass Ablated Δ µgms	Velocity V_f Kilometer/sec.	Impulse $M_f V_f$ dyne-sec.	Effective Exhaust Velocity C Kilometer/sec.
WP #22 (gun)	Ti	5 cm	(Cylinder in 6 mm gun barrel)		179 µgms	172.5 µgms	6.5 µgms	0.079	1.36	2.1
WP #23	Ti + LiH	5 cm	(Cylinder in 4 mm gun barrel)		49.2 µgms	--	--	0.22	1.08	--
WP #24	Fe	5 cm	(Cylinder in 4 mm gun barrel)		94.2 µgms	93.0 µgms	1.43 µgms	0.119	1.11	7.8
WP #25	Fe	5 cm	(Cylinder hit on disk)		179 µgms	175 µgms	4.4 µgms	0.084	1.47	3.3
WP #26	Fe	5 cm	Flat cylinder (hit on side)		88.4 µgms	87.4 µgms	1.1 µ ms	0.129	1.13	10.3
WP #27	Fe	5 cm	Flatten cylinder (hit on side)		55.2 µgms	53.4 µgms	1.8 µgms	0.20	1.07	5.9
WP #28	Fe	5 cm	Flatten cylinder (hit on side)		44.4 µgms	42.7 µgms	1.7 µgms	0.22	0.94	5.5

TABLE V-1

Q-SWITCHED (3 JOULE - 100 NANOSECOND) LASER INDUCED EFFECTIVE EXHAUST VELOCITIES VIA ACCELERATION OF FREE PARTICLES

Code	Material	Lens focal length cm	Initial Shape	Initial Diameter microns	Initial Mass M_o µgms	Final Mass M_f µgms	Mass Ablated µgms	Velocity V_f Kilometer/sec.	Impulse $M_f V_f$ dyne-sec.	Effective Exhaust Velocity C Kilometer/sec.
WP #3	Ti	5 cm	Cylinder	not measured	75.0 µgms	73.0 µgms	2.0 µgms	0.16	1.17	5.7
WP #4	Ti	5 cm	Cylinder	264	110.7 µgms	108.8 µgms	1.9 µgms	0.12	1.31	6.8
WP #5	Ti	5 cm	Cylinder	not measured	21.8 µgms	19.9 µgms	1.9 µgms	0.41	0.82	4.1
WP #6	Ti	5 cm	Sphere	143	6.8 µgms	4.5 µgms	2.3 µgms	1.05	0.47	2.6
WP #8	Ti	2.75 cm	Cylinder	not measured	94.6 µgms	92.2 µgms	2.4 µgms	0.16	1.48	6.1
WP #9	Ti	2.75 cm	Cylinder	not measured	51.7 µgms	no fragments found		1.07	--	--
WP #10	Ti	2.75 cm	Cylinder	not measured	83.8 µgms	80.0 µgms	3.8 µgms	0.18	1.44	3.7
WP #11	Ti	5 cm	Cylinder	258	35.8 µgms	33.4 µgms	2.4 µgms	0.33	1.10	4.3
WP #12	Ti	5 cm	Cylinder	321	59.6 µgms	55.5 µgms	4.1 µgms	0.236	1.31	3.1
WP #13	Ti	11 cm	Cylinder	not measured	78.1 µgms	77.5 µgms	2.65µgms	0.12	0.93	3.5
WP #14	Ti	11 cm	Cylinder	not measured	36.1 µgms	33.2 µgms	2.9 µgms	0.26	0.86	2.9
WP #15	Ti	11 cm	Cylinder	not measured	58.2 µgms	55.7 µgms	2.55 µgms	0.130	0.72	2.9
WP #16 (beam	Ti	5 cm	Cylinder	not measured	103.4 µgms	101.3 µgms	2.1 µgms	0.113	1.15	5.5
WP #17	Al	11 cm	Cylinder		142.2 µgms	140.5 µgms	1.7 µgms	0.113	1.60	9.4
WP #18	Ti + Carbon*	11 cm	Cylinder with carbon dab		159 µgms	--	--	0.076	~1.21	--
WP #19	Ti + C	5 cm	"		128.7 µgms	125.1 µgms	3.8 µgms	0.107	~1.34	3.5
WP #20 (gun)	Ti	5 cm	(Cylinder in 1 mm gun barrel)		80.4 µgms	75 µgms	5.5 µgms	0.147	1.10	2.0
WP #21	Ti	5 cm	(Cylinder in 1 mm gun barrel		62.2 µgms	--	--	0.210	1.31	--

as measured with the reed vibrator, the final mass as measured with the reed vibrator, the final mass as measured with the reed vibrator, the mass loss (i.e., difference between the preceding columns), the velocity of the accelerated fragment, the momentum of the fragment, and finally the effective exhaust velocity as computed from the rocket equation (equation I-1).

After acceleration the particles were placed in separate plastic containers for later examination with a microscope. Figure V-3 shows front, side, and rear microphotographs of "weighed particles" #3, 4, and 5 after acceleration. The first two particles were cut from nominally 0.012 inch diameter titanium wire, while the latter was cut from some wire etched down to 0.004 inches in a 30% solution of hydrofluoric acid in nitric acid. Note the mushrooming of the smaller particle indicating that the acceleration forces were near the yield point.

Figure V-4 shows microphotographs of titanium cylinders originally cut from 0.012 inch wire (i.e., weighed particles #8 and 10) and accelerated by radiation focused through a 2.75 cm focal length lens. The higher power densities resulted in greater yielding of the bulk matter, even to the extent that fragments were dislodged from the lip of the particle. As a result, the effective exhaust velocities listed in the last column of Table V-1 could well be in error due to the fragmentation of the particles under the more intense laser beam.

Figure V-5 shows a two-side view microphotographs of an originally spherical particle (i.e., W.P. #6) after it had been a accelerated in vacuum. The flattened shape of the fragment shows that the particle had been subject to forces close to yield point of the material.

Some composite particles were also tested, in particular particle #18, 19, and 23 in Table V-1. The former two particles were prepared by coating the ends with Aquadag (i.e., colloidal carbon) in an attempt to combine the strength of titanium with the low atomic weight of carbon. The result was not particularly better than with the pure particles. A particle of titanium coated with lithium-hydride (i.e., #23) was no better.

Front Side Rear

Weighed Particle #3

Front Side Rear

Weighed Particle #4

Front Side Rear

Weighed Particle #5

Figure V-3: Microphotographs of three of the titanium cylinders (listed in Table V-1) after they had been accelerated in vacuum by the focused radiation from the 3 joule, 100 nanosecond laser, removed from a paraffin target and washed in trichlorobenzene. The particles were struck on the surface marked rear. Note the mushrooming of the smaller particle.

Front Side Rear

Weighed Particle #8

Front Side Rear

Weighed Particle #10

Figure V-4: Microphotographs of Particles #8 and 10 of Table V-1 after being accelerated into the paraffin piezoelectric time of flight detector. The energy from the laser was focused with 2.75 cm focal length lens and was more concentrated than in previous microphotographs The accelerating forces were closer to the yield strengths of the material. The photographs indicate that fragments were torn off.

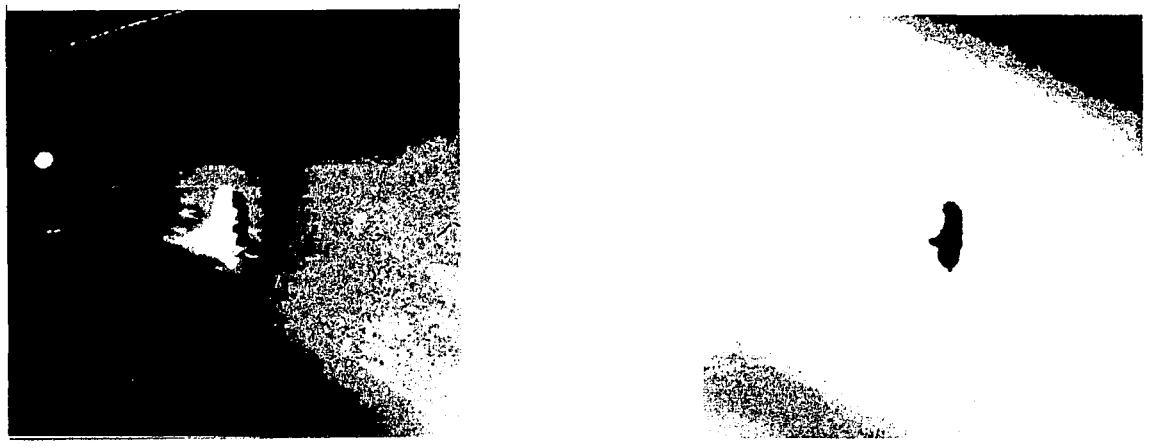

Figure V-5: Two microphotographs of the side view of an originally 143 micron diameter spherical titanium particle accelerated in vacuum by the 5 cm focused radiation from a Q-switched ruby laser. Particle is Weighed Particle #6 on Table V-1.

The gun barrel approach was also tested in an attempted to learn whether the presence of confining walls would aid to better couple the plume to the particle. Reference to W. P. #21 will show that the final velocity was actually no better than a freely accelerated particle of the same mass.

The one test with aluminum gave a rather surprising and impressive result with a measured effective exhaust velocity of magnitude close to that needed for the acceleration to meteoric velocities. The result was surprising, particularly in relationship to rather low exhaust velocities measured on larger samples earlier in the program.

Iron particles cut from wire gave some good velocities, but too low for acceleration to velocities in the 20 kilometer per second range.

The results discussed in this chapter are the culmination of the program; namely, the measurement of the effective mechanical exhaust velocities.

CHAPTER VI
SUMMARY AND RECOMMENDATIONS

The present program has been concerned with the feasibility of accelerating small typically 100 micron sized particles to meteoric velocities of the order of 20 kilometers per second via the focused radiation from a high intensity pulsed solid state laser system.

After exploratory experiments with ballistic pendulums and large test samples using various pulsed laser sources, effort was concentrated on the Q-switched mode since this gave the highest peak power and permitted operation at the threshold of material yield strengths.

The program lead to the development of a method of computing the effective exhaust velocity directly from experimental values of the initial mass, final mass, and the terminal velocity of test particles accelerated in vacuum by the focused radiation from a 3 joule - o.1 microsecond duration Q-switched laser system. The initial and final mass of each test particle was determined by a mass measurement apparatus (also developed under the program) which is based upon the change in the resonant frequency of an electrically maintained Elinvar reed. The reed weighing apparatus had a range of 2 - 100 micrograms, a sensitivity of 0.1 micrograms, and an accuracy of 1% for particles of mass at the heavy end of its range.

The values of the effective exhaust velocities measured by the aforementioned approach could then be used to predict via the rocket equation the ratio of the amount of mass which would have to be ablated to take a given particle from rest to a terminal velocity of 20 kilometers per second. Thus, through the experimentally measured values of the effective exhaust velocity the feasibility of the laser approach could be assessed as a means of achieving or simulating meteoric velocities.

Titanium metal was given the greatest attention and was found to have an effective exhaust velocity of 4-6 kilometers per second when subject to the radiation from a 3 joule - 0.1 microsecond beam from a Q-switched ruby laser focused with a 5 centimeter focal length simple lens.

In addition, the tests established that the material was being subject to forces close to its yield strength as judged from microscopic examinations of the accelerated fragments.

Taking the value of 6 kilometers per second as the best effective exhaust velocity of titanium metal, one then computes from the rocket equation an initial to final mass ratio of 0.0358. That is to say, 96.4% of the original particle would have to be burned away to bring the remaining mass up to a velocity of 20 kilometers per second. Such a burning ratio is too extreme to believe that enough experimental control could be maintained to yield an intact final accelerated fragment.

Iron had an effective exhaust velocity of 5 kilometers per second when subject to the same Q-switched ruby laser beam. Like titanium, the exhaust velocity was too low for its eventual acceleration to a terminal velocity of 20 kilometers per second. Aluminum had an effective exhaust velocity of 9 kilometers per second, only a factor of two off the value believed necessary to accelerate this material to 20 kilometers per second. The high effective exhaust velocity of aluminum was discovered late in the program and was inconsistent with earlier measurements in the regular and intermediate lasing mode.

The program established that ductile materials of low density and low atomic weight yielded the highest effective exhaust velocities when subject to the radiation from a Q-switched laser oscillator - amplifier system.

Although the experimentally measured effective exhaust velocities were not large enough to accelerate matter to terminal velocities of 20 kilometers per second, the program did show that the laser ablation approach is quite feasible as a means of generating particles with velocities in the 10 kilometer per second range.

The effective exhaust velocities which were measured are not small, and in the case of aluminum, titanium, and iron correspond to energies of approximately 10 volts per atom or thermal temperatures of 100,000^{o}K. Since the experimental values of the exhaust velocities are time averages over all of the ejected material the values are impressive.

Within the scope of the program, it is therefore concluded that final velocities (20 kilometer per second) are not feasible when matter is ablated by the focused radiation from a pulsed laser system, but that velocities in in the 1-10 kilometer range are feasible. The investigators recognize that through the laser acceleration approach, 20 kilometer per second particles may possibly be produced; however, as a result of the present study the investigators conclude that there is no straightforward charted course to the realization of this goal.

APPENDIX I

THE MASS MEASUREMENT TECHNIQUE

In order to determine the effective exhaust velocity and hence determine the ultimate feasibility of the laser acceleration approach, it was necessary to measure the amount of mass lost by ablation.

The first measurements were made with commercial laboratory balances.* The sensitivity limit of these balances, about 20 micrograms, proved adequate for tests with the regular lasing mode, but not for the Q-switched mode. Operation in the Q-switched mode is of particular significance because there the laser power densities approach the ultimate values leading to the expectation of maximum exhaust velocities. The power densities available from the Q-switched mode gives forces of the order of the yield strength of the strongest materials and thus tests in the Q-switched mode are tests at the maximum feasible power density.

In an early set of tests, the mass loss from Q-switched operation was obtained with the commercial balances by taking about 100 shots on a flat block and weighing before and after. While this gave a measure of the average mass loss, 2 micrograms per shot for titanium, visual examination of the pits showed significant variation in size. Another weakness of the many shot technique was that it was limited to flat plate geometry of not too small size.

As a consequence of this need to measure the mass loss from a single shot on small diameter specimens, a special instrument was developed. The final version, which is capable of weighing 10 microgram particles to an accuracy exceeding 0.1 micrograms and 100 microgram particles to an accuracy of 1 microgram, is shown schematically in Figure 1-IA. A photograph of the actual mass measuring reed vibrator is shown in Figure 2-IA.

The basic operation is as follows: The instrument is basically an oscillator, the frequency of which is determined by the natural frequency of a small reed. The addition of a particle to the end of the reed decreases

*Mettler Model M-5 Microbalance was one of the balances used.

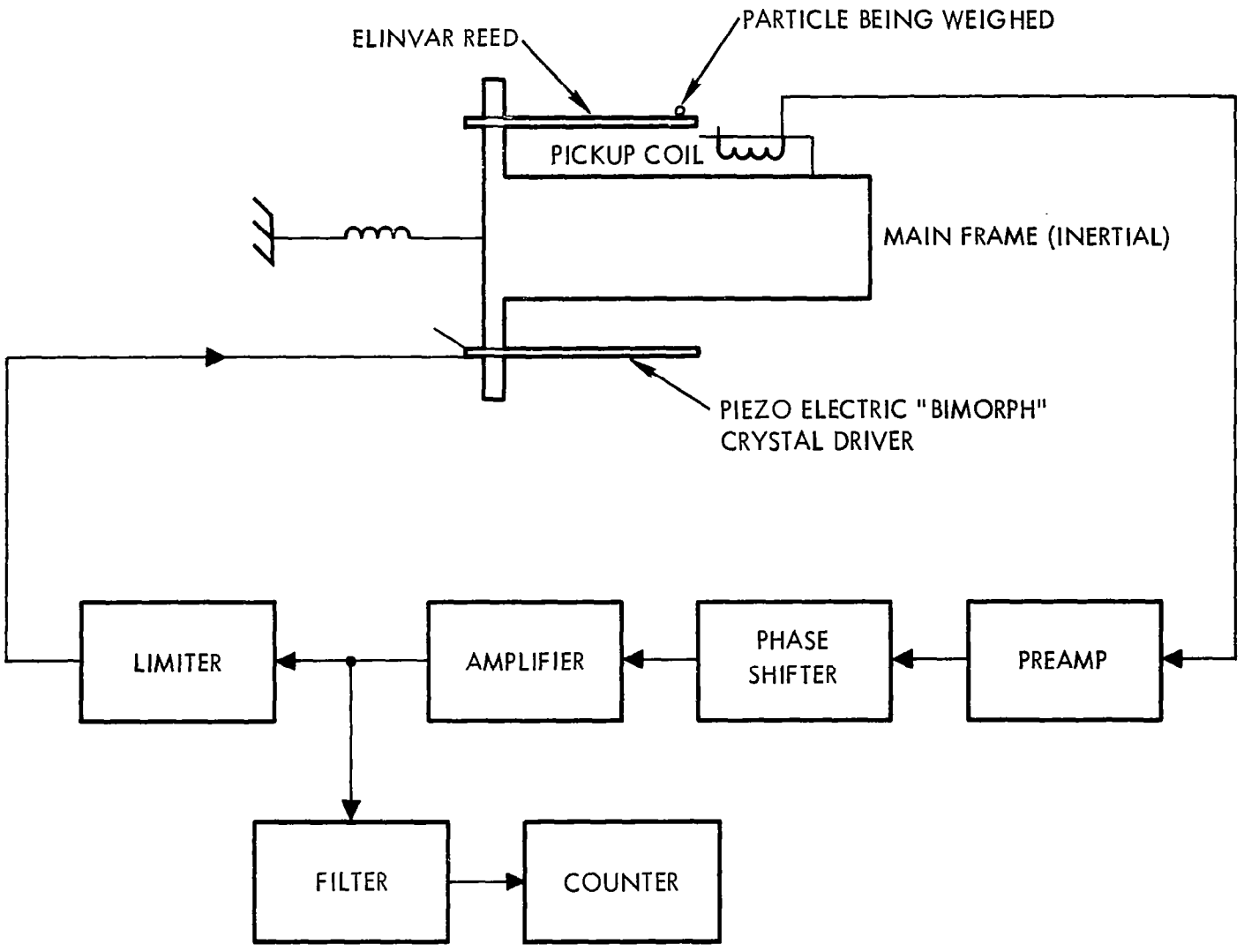

Figure 1-IA. Schematic of the Reed Vibrator Microgram Measuring Apparatus

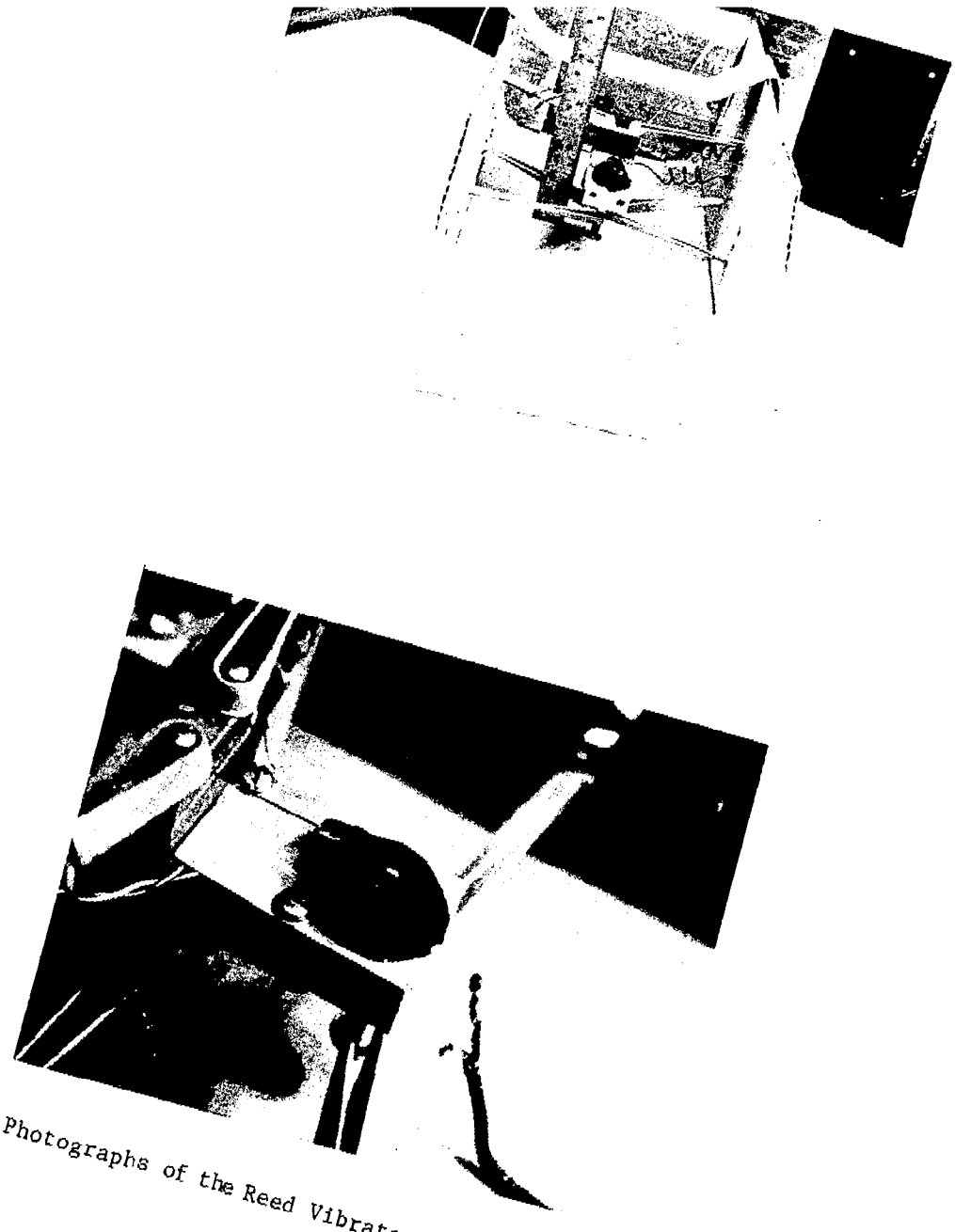

Figure 2-IA. Photographs of the Reed Vibrator Mass-Measuring Apparatus

its natural frequency in proportion to the mass of the particle. A digital counter measures the oscillator period, averaged over 3000 cycles. The difference in period before and after adding the particle, multiplied by a calibration constant, gives the particle mass.

The particle is caused to adhere to the reed by the presence of a minute film of Apiezon N vacuum grease on the end of the reed. For this reason, a weighing is made from the difference of periods before and after adding a particle, the period typically shows that 0.1μ gram or less of grease has been removed with the particle. This unconventional use of grease in connection with a microbalance is perfectly acceptable because of the samll size of the surfaces involved.

The heart of the instrument is the Elinvar reed made by the Hamilton Watch Company. Its dimensions are 19mm x 0.5mm x 0.16 mm and the natural frequency is 324 cycles per second. Elinvar is analagous to Invar; however, in Elinvar it is the elastic coefficient that is made insensitive to temperature. The use of Elinvar for the reed renders the instrument insensitive to temperature variations. Earlier versions of the reed-mass-measuring apparatus made at the beginning of the program, using conventional clock balance wheel springs, had frequency variations due to temperature fluctuations which prevented adequate sensitivity from being achieved.

The vibration of the Elinvar reed is detected via a small coil sensing the residual magnetism of the Elinvar. This signal, about 300 microvolts, is amplified, phase shifted, limited and then used to drive a ceramic "bimorph" crystal attached to the main frame. The vibration of the ceramic crystal produces a minute vibration of the main frame, suspended by rubber bands to the main mounting frame. This minute vibration of the main frame causes the Elinvar reed to vibrate when the vibration is at the natural frequency of the reed. The amplitude of vibration of the Elinvar reed is about 30 microns and is held to a very constant value during the measurements.

Small amplitude of vibrations are desired, since the acceleration of the particle being weighed is small, thereby minimizing the attachment forces necessary to keep it onto the reed.

The bimorph crystal consists of two thin ceramic crystals of lead zirconate titanate bonded to each other along their entire length.[+] The two components are oppositely polarized so that when a voltage is applied, one crystal expands while the other contracts, resulting in microscopic bending of the crystal unit. Each face of the crystal is coated with silver which serves as an electrode. There is also a silver electrode between the two crystal pieces, but this is used only in the initial polarization of the crystals. "Bimorph crystals" are the electrostatic analog of the bimetallic strips used in temperature sensing equipment.

The dimensions of the crystal used are 32mm x 13mm x 0.6mm. The mounting clamp at one end reduces the vibrating lengths by 6mm.

The natural frequency of the bimorph was adjusted to be the same as the frequency of the Elinvar reed by adding mass (clay) to the free end of the unclamped crystal, thereby lowering the amount of drive power required to keep the reed in oscillation. Further, since the Q of the ceramic bimorph is far lower than the Q of the Elinvar reed, the frequency of oscillation is almost completely controlled by the Elinvar and the change in frequency with mass remains linear over the present range of interest.

The electrical analog of the mechanical vibrator assembly is simply a double tuned coupled circuit (shown schematically in Figure 3-IA). The Q of the input tuned circuit is low corresponding to the low Q of the cystal driver. The Q of the output resonant circuit is very high corresponding to the high Q of the Elinvar reed. The coupling coefficient between the resonant circuits is determined by the inertia of the main frame. In the constructed version the mass is sufficiently large so that the assembly operates well below critical coupling as determined by plotting the output response for a constant amplitude swept frequency input.

The dimensions of the principle piece of the main frame are 5cm x 2.5cm x 1.25cm. The material is aluminum.

[+]The bimorph crystals were home-made and were supplied to the authors by C. Knox of this laboratory.

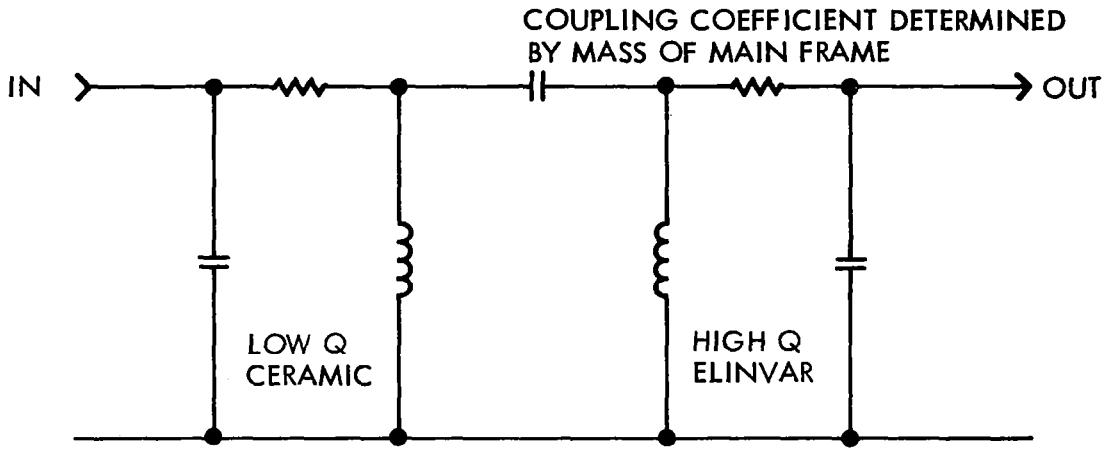

Figure 3-IA. Electrical Analogue Circuit of the Vibrating Reed Mass Measuring Apparatus

We shall now describe some of the details of the elements of the block circuit diagram shown in Figure 1-IA. The purpose here is partly to provide a record. No claim is made that the components were optimally designed. On the contrary, the instrument was assembled using equipment on hand which would do the job rather than by building specialized electrical components.

Both amplifiers are battery operated transistor audio amplifiers. The preamplifier has a voltate gain of 500. The output amplifier has a voltage gain of 70. The output required is only 4 volts peak to peak into 1000 ohms.

The phase shifter circuit is shown below in Figure 4-IA.

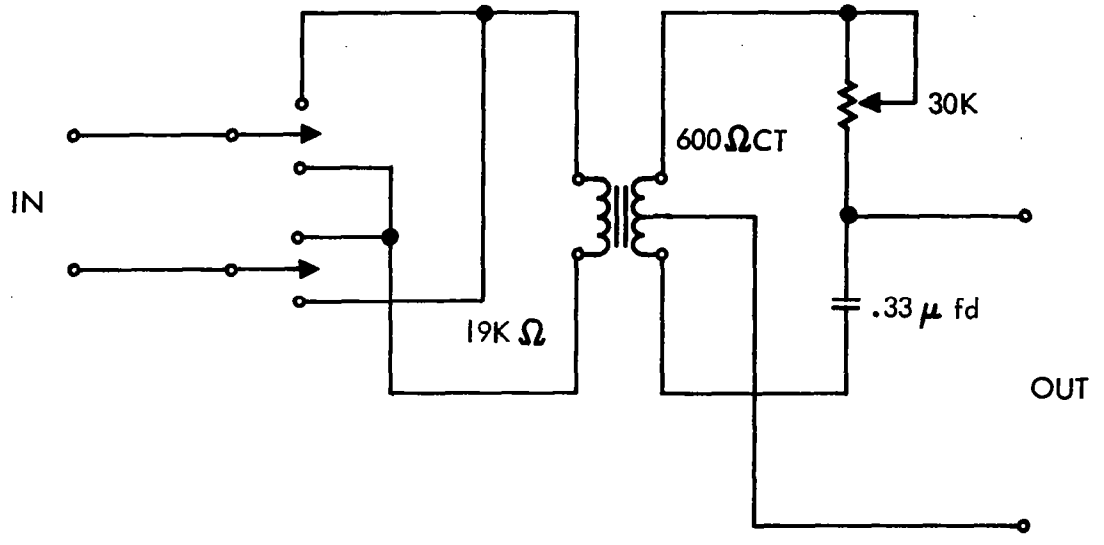

Figure 4-IA: Schematic of Phase Shifter Used in the Reed Vibrator Mass Measuring Apparatus Shown in Fig. 1-IA.

This circuit introduces a voltage loss of 11. The circuit is unnecessarily elaborate for a finished device because once the phase is properly set it never needs to be changed. The above circuit was on hand and was convenient during development, for it shifts the phase without changing the gain.

The limiter consists of two silicon diodes in parallel so the voltage driving the crystal is limited to about 1.4 volts peak to peak.

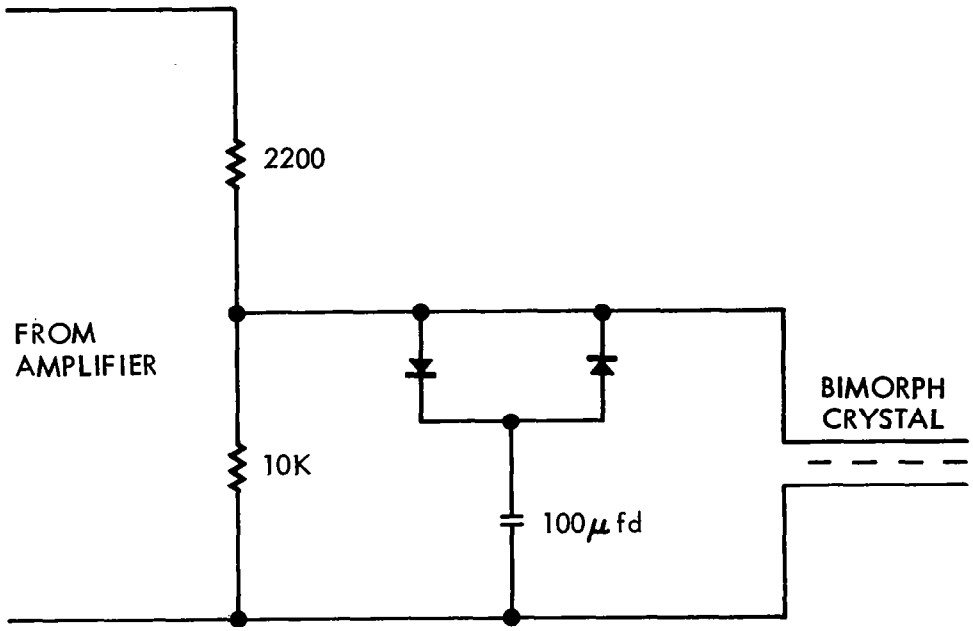

Figure 5-IA: Schematic of Limiter in the Reed Vibrator Circuit

The function of the limiter is to set the amplitude of vibration. A small amplitude of vibration as noted earlier is desirable since it reduces the required attachment forces. A constant amplitude is desirable to reduce or eliminate frequency shifts due to non-linearities of the elastic constant of the vibrating reed (in particular, due to the magnetic force from the "mu" metal core in the pickup coil). With a given limiter the amplitude can be controlled over a small range by the amplifier gain control. In operation the vibration was adjusted to the same level before each reading was taken.

The filter is a simple LC tank tuned to the reed frequency.

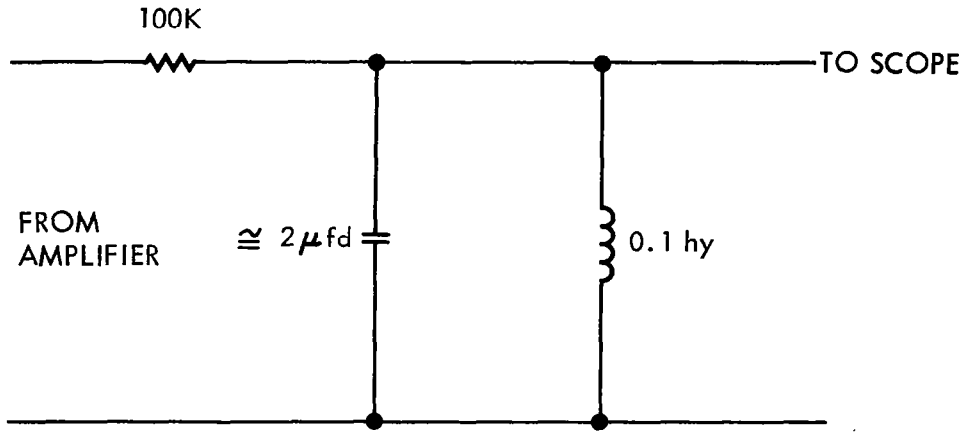

Figure 6-IA: Schematic of the Filter in the Reed Vibrator.

Its function is to remove most of the transistor noise by limiting the band width before the signal enters the counter.

It was found that feeding the signal to be counted, first to a 545 Tektronics oscilloscope and then running the counter from the + gate output of the oscilloscope, resulted in the most noise free counting. Apparently for these low frequency signals,at the volt level,the 545 has triggering circuits superior to those of the counter. The counter was arranged to count its internal standard for 3000 periods of the reed.

The instrument was calibrated by weighing a known mass. The calibrating mass was prepared by weighing a length (typically several meters) of fine copper wire on a conventional balance and then cutting from it (typically several millimeters) with a sharp razor the calibrating mass. The mass of the calibration weight was calculated from the ratio of the lengths and was typically 120 micrograms.

The calibration of the instrument as well as its linearity was separately checked by weighing small spheres of titanium. The mass of these spheres was calculated using published values for the density of titanium and multiplied by the volume calculated from the diameter measured with a microscope with a filar eyepiece.

The calibration constant was further calculated from the mass, geometry, and period of the reed using solutions found in textbooks.* The value obtained was within 1% of the experimental value. Such agreement appears to be fortuitous!

The experimental constant of the reed-micromass measuring apparatus was 1380 microseconds per microgram (i.e., 1380 us/ug) when counting for 3,000 periods. The duration of 3,000 periods was approximately 9,200,000 microseconds or 9 seconds. The count interval was chosen as a compromise between measurement time and sensitivity. The count uncertainty is normally less than $\pm$ 50 microseconds, which to first approximation is independent of the count.

*N. W. McLachlan, Theory of Vibrations, Dover Publications, 1951, p. 111.

The count uncertainty appears to be due to residual noise, probably originating in the input transistor. For the count duration of 3,000 periods, the count uncertainty of ± 50 microseconds amounts to $\pm .036$ micrograms uncertainty.

For masses in the 10 microgram range this count uncertainty is the principle source of error. However, for masses on the order of 100 micrograms the primary source of error is the positioning of the particle on the reed. Repeated weighing of the same 100 microgram irregular shaped particle gave results differing by about 1 microgram.

The following data are rather typical of operation of the microbalance and are included to illustrate to the reader the method of measurements during this study:

Weighed Particle Number 6

Titanium sphere, 143 microns diameter.
Weight calculated from diameter, 6.9 micrograms.
The numbers listed below give successive counts of the number of microseconds in 3,000 periods of the reed.

Reed empty
9,241,509 μsec
9,241,499 μsec
9,241,527 μsec
9,241,523 μsec

Sphere on reed
9,250,613 μsec
9,250,596 μsec
9,250,592 μsec
9,250,594 μsec

The change is 9080 μs which corresponds to 6.6 μg. The particle was then accelerated with the laser and caught in the paraffin coating of the time of flight censor. After solvent cleaning of the main accelerated fragment the following readings were obtained:

Reed empty

9,241,427 μsec

9,241,346 μsec

9,241,425 μsec

9,241,371 μsec

Fragment on reed

9,247,390 μsec

9,247,406 μsec

9,247,422 μsec

9,247,418 μsec

The change is 6017 μs which corresponds to 4.4 μg.

For completeness, we include here the other data for this particular particle. The arrival at the impact sensor is shown in the oscillogram reproduced in Figure 7-IA. The main fragment arrived at 76 μs (sweep speed was 20 μs/cm). The signal which starts at the beginning is due to laser radiation on the impact sensor. The flight distance was 8cm, hence the velocity was 1.05 km/sec. The effective exhaust velocity, which includes other fragments as part of the exhaust, was in this case

$$C = \frac{v}{\ln \frac{M_o}{M_f}} = \frac{1.05}{\ln \frac{6.6}{4.4}} = \frac{1.05}{.406} = 2.6 \text{ km/sec.}$$

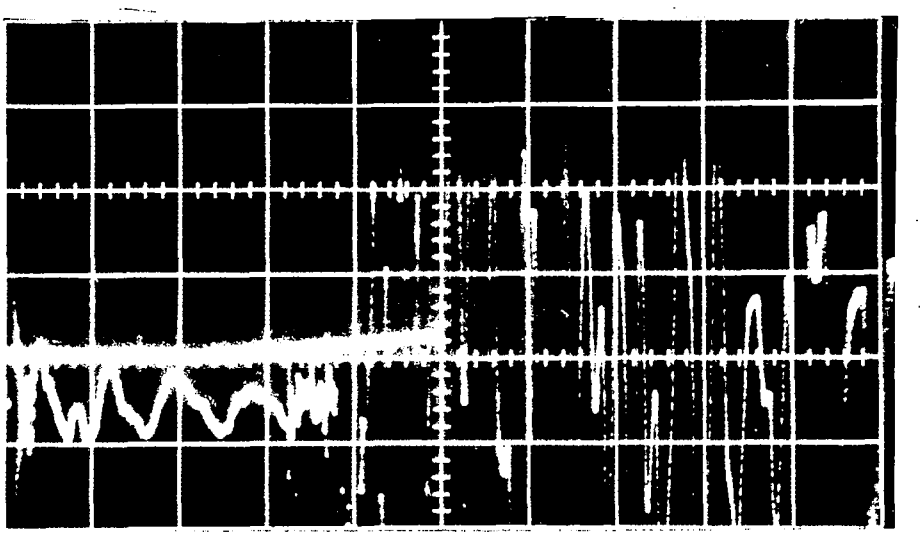

Figure 7-IA. Oscillograph recording of the output of the vacuum mounted paraffin coated piezo-electric sensor when struck by "weighed particle No. 6," accelerated by radiation from Q-switched ruby laser. Vertical scale is crystal output, horizontal sweep speed 20 microseconds per major division. Main fragment struck at 76μsec (smaller fragment at 65 μsec). Range length was 8 centimeters. Thus velocity of major fragment was 1.05 kilometer/second.

Conclusion

The microbalance described above was adequate to perform the required measurements for the particle acceleration program. The instrument is quite easy to use. It should be emphasized that the improvement of the device was terminated as soon as it was adequate for the needs of the present program. It is the opinion of the investigators that the device can be still further improved and may find more general use. Operation of the reed in the second mode of vibration with the particle at the antinode nearest the clamp should remove the sensitivity to particle position. The use of low noise transistors and an improved pickoff should give even further improvements in sensitivity.

APPENDIX II

PULSED SOLID STATE LASERS

At the inception of this program, the Physical Electronics Laboratory of TRW Systems had sufficient equipment to assemble a wide variety of pulsed solid state laser systems. These included a $\gtrsim$30 joule -1 millisecond duration ruby and neodymium doped glass lasers; a 20 joule ~ 60 microsecond either ruby or neodymium doped glass laser, pumped by a fast annular lamp; and a Kerr cell switched ~1 joule - 50 nanosecond Giant Pulse laser oscillator.

Only the intermediate pulse laser and the giant pulse laser were of interest to the present program, the former because it had emission times comparable to those expected for the acceleration of matter, and the latter because it emitted radiation at the limiting or ultimate power densities and could thus be used to verify that focused optical radiation could indeed exceed the yield strengths of materials and could achieve effective exhaust velocities of interest. Since these questions were the key to feasibility, the bulk of the experimental work was done with the giant pulse laser system.

This section will describe in sufficient detail the solid laser systemsused in the present program.

I. Giant Pulse Ruby Laser Oscillator-Amplifier System

The Q-switch ruby laser oscillator consisted of a 1/2-inch x 3-3/4-inch - 60° cylindrical ruby laser rod mounted within a helical xenon flash lamp and a concentric polished aluminum reflector. The three components were mounted separately in an air cooled aluminum housing which in turn carried the input and exit air cooling lines and the connection to the 5 K.V.-360μF flash lamp capacitor bank. The "laser-rod-lamp" housing was clamped in turn onto a 6-foot long machined I beam. On to this I beam was also attached a calcite Glan polarizing prism, a nitrobenzene Kerr cell, and the dielectric coated plane end reflectors. The Kerr cell and polarizing prism were placed between the 99% end reflector and the ruby laser rod,

and were arranged so that with 19.5 KV quarter wave bias on the Kerr cell, the 99% reflector was isolated from the laser rod. The other or output reflector had a 35% reflective coating which optimized the integrated emission from the laser system. The two end mirrors were separated by 1.5 meters in order to realize maximum power density and minimize beam divergence as well as the erosion of windows and surfaces under the extreme optical power density generated by the laser.

A "giant pulse" is generated by pumping the laser rod to a high degree of inversion with the xenon flash lamp. At the end of the pump lamp period (typically 1 millisecond) the terminals of the electrically biased Kerr cell are short circuited by a fast thyration. The "supercharged" ruby is effectively placed in the optical resonator and energy stored in the excited fluorescent levels of the chromium ions is converted into radiant energy in times of the order of ten times the light transit time between the end reflectors.

The Q-switched laser oscillator was conventional except for the incorporation of a ruby rod of high optical quality*, and the use of a large (~1.5 meter) mirror separation.

Tests verified that with large mirror separation and apertures before the end reflectors, of diameters slightly less (~7/16 inch) than that of the rod, the output beam from the laser asymptotically approached the diffraction limited value. The emission (see Figure 2-IIA) was a single optical pulse of approximately 100 nanosecond duration and 1 joule total energy of wavelength 0.6943 microns.

The output of the Q-switched oscillator was further enhanced by the addition of a power amplifier consisting of a 1/2-inch x 3-3/4-inch - 90° ruby laser rod within a helical xenon flash lamp. The power amplifier head was placed before the output reflector and when pumped to saturation served to triple the output of the oscillator.

*Product of Linde Division, Union Carbide Corporation; a Twyman Green interferogram supplied by manufacturer showed a maximum variation in optical path length along the length of the rod of six wavelengths across the rod's diameter.

The complete Q-switched laser oscillator-amplifier is shown schematically in Figure 1-IIA. Figure 2-IIA shows an oscillogram of the output of the oscillator alone recorded with a biplanar photodiode, a Tektronix 519 traveling wave oscilloscope and a Tektronix C-12 (f/1.9, 1:0.5) oscilloscope camera. The emission from the oscillator-amplifier system was plane polarized with the electric vector perpendicular to the c-axis of the laser rods. For peak performance, both rods were oriented with their c-axis in the same plane and at 90^{o} to the axis of the calcite polarizer. Figure 3-IIA shows the tested performance of the Q-switched oscillator separately and with its output enhanced by the power amplifier. The amplifier's flash lamp was timed to fire 0.32 milliseconds after the initiation of current through the oscillator's flash lamp, while the Kerr cell in the oscillator was programmed to open at 0.95 milliseconds.

The potent nature of the emission from the above laser oscillator-amplifier is illustrated in Figure 4-IIA by the photograph of the air breakdown at the focus of a simple lens of 5 centimeter focal length. Breakdown could occasionally be realized with lenses of even 9.6 centimeter focal length; however, in this case the alignment and cooling of laser crystal was most critical. Air breakdown was attended by a report similar in sound and intensity to that of a .22 caliber rifle. This simple test was repeatedly used throughout the program to test the operability of the Q-switched laser system. Failure to breakdown air indicated that the system had either drifted out of alignment or that the internal optical surfaces (most particularly those of the Kerr cell) had accumulated dust and become less transparent, thereby lowering the Q of oscillator and degrading the emission. Air breakdown was an ideal fitness test for this very versatile and reliable laser system.

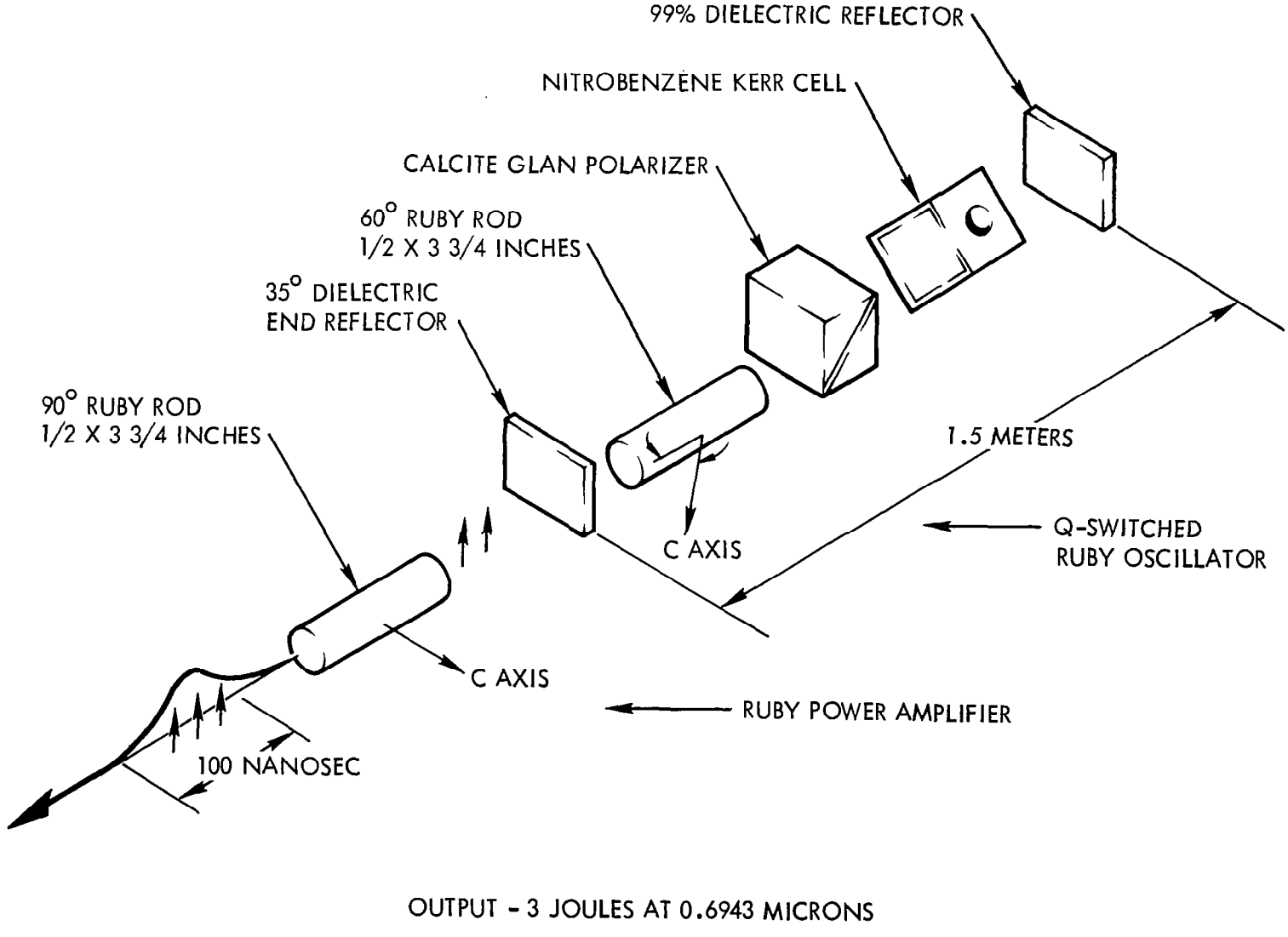

Figure 1-IIA: Schematic of Q-switch Ruby Laser Oscillator-Amplifier whose focused output was used to study and accelerate matter in vacuum. Not indicated are the helical xenon pump lamps and reflectors around the two rubies.

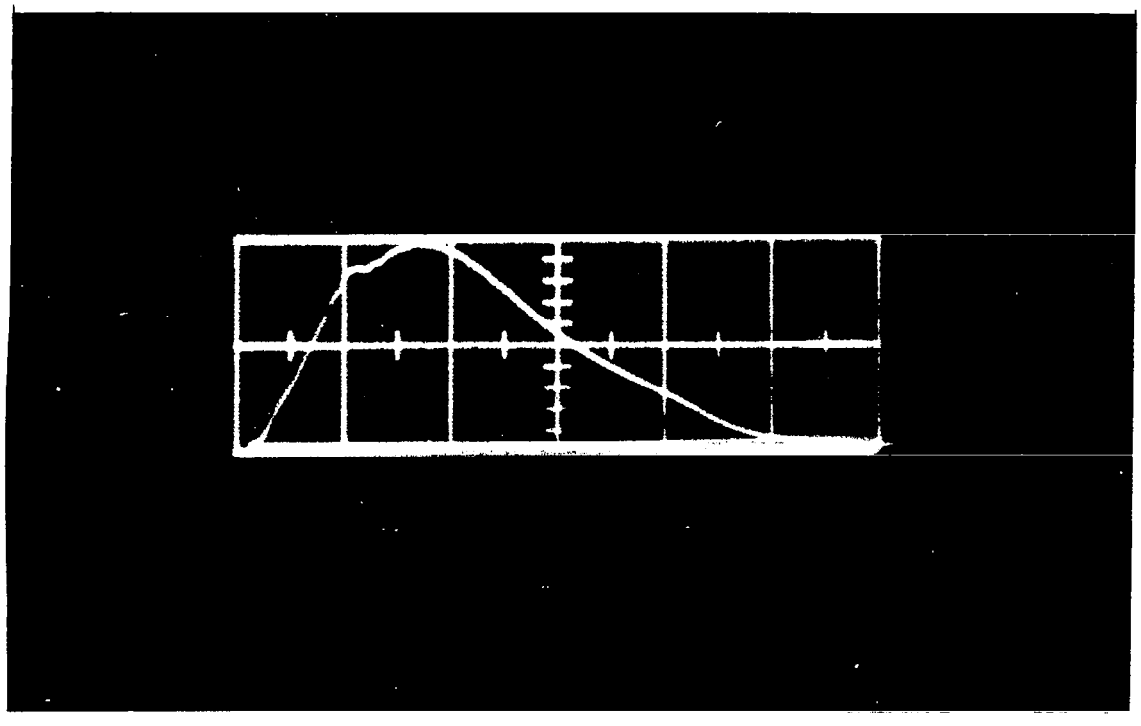

Figure 2-IIA: Sample photoelectric oscillogram of the 0.6943 micron emission from the Q-switched giant pulse oscillator shown in Figure 1-IIA. Vertical sensitivity, 4 megawatts per major division; horizontal sensitivity, 50 nanoseconds per major division.

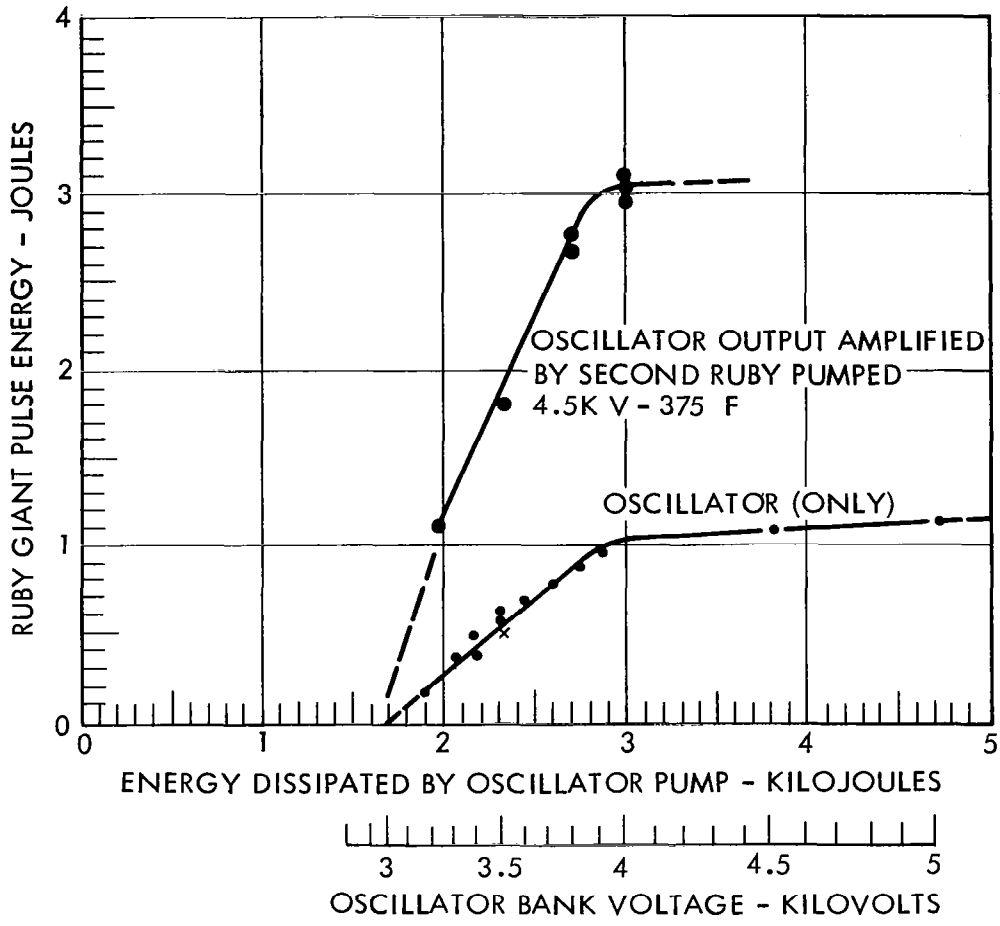

Figure 3-IIA: Performance of giant pulse laser oscillator having 1/2" x 3-1/2" ruby rod and 99% and 35% end reflectors separated by 1.5 meters Also shown is the amplification by a second 1/2" x 3-3/4" ruby rod pumped at constant 3.8 KJ input. Amplifier lamp started 0.32 millisecond after initiation of oscillator pump current. Oscillator Kerr cell opened 0.95 millisecond after initiation of pump current.

Figure 4-IIA: Photograph of Air Breakdown at Focus of Simple 5.5 centimeter focal length lens by the 3 joule ~100 nanosecond Emission from the Ruby Oscillator-Amplifier Laser System shown schematically in Figure 1-IIA. The housing with the amplifier rod is to the left, clamped to the I beam

II. Intermediate Pulse Laser

The second laser system was of particular interest to the present laser acceleration program due to the fact that it had an emission or lasing duration of the same order as the times required by theory to accelerate matter to meteoric velocities without their crushing under inertial stress.

The intermediate laser system was developed and built in 1964 under an Air Force Contract (i.e., AF 33 (615)-1072) for the fast excitation of 5/8 x 8-inch long solid state laser rods. At the initiation of the present program the laser system had to be completely rebuilt. In reassembling this system, the high current bus bars, charging lines, charging resistors, interlocks, discharging resistors, etc., were completely rebuilt and arranged so that all components were surrounded by a grounded aluminum cover. In addition, the covering sheets were lined with 1-inch thick felt and all cracks between the individual 250μF capacitors in the 12 unit bank were filled with modeling clay. These latter improvements served to protect operating personnel from the explosive forces generated by the accidental failure of any of the insulators on the 38,000 joule capacitor bank.

The intermediate laser is based upon a "fast" annular flash lamp of extreme strength, having an outer wall consisting of alternate disks of quartz and graphite lined aluminum. The inner wall is a quartz tube, within which is placed the laser rod, and which is under compression when subjected to the pressures generated by the electrical discharge. The outer wall is massive and is segmented so that flaws or cracks will not propagate. The light producing electrical discharge flows between the annular space defined by the inner quartz tube and the segmented outer envelope wall. Ballast chambers on either side of the end electrodes serve to catch the products of ablation as well as moderate the gas pressure during the discharge.

Figure 5-IIA shows a photograph of the reassembled lamp with one of the side covers removed. The segmented annular lamp is mounted above the 5 K.V. - 3,000μF (38,000 joule) capacitor bank (i.e., twelve - 250μF fast capacitors). Over the lamp a heavy aluminum beam is mounted, carrying the

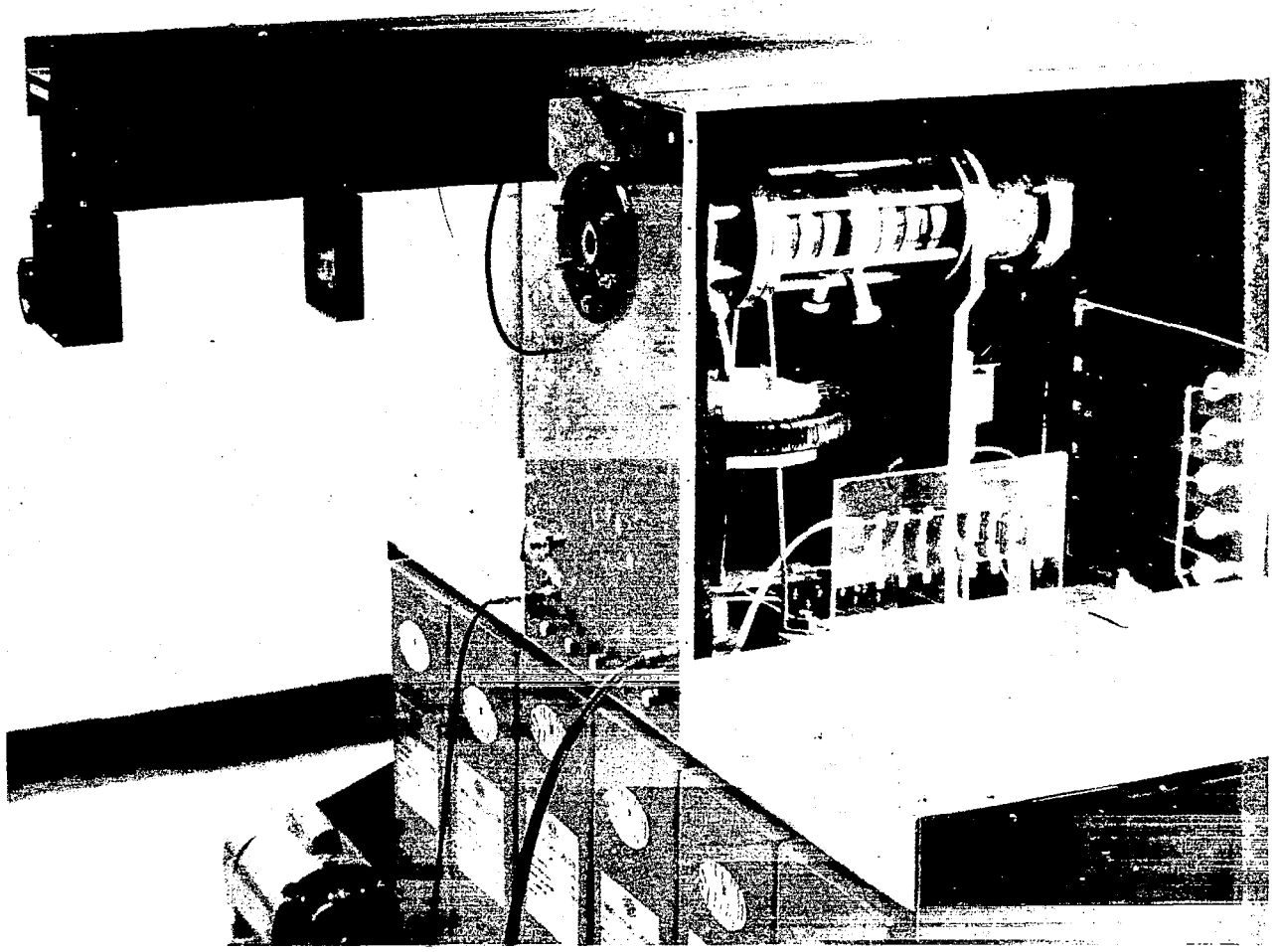

Figure 5-IIA: Photograph of the Intermediate (~50 microsecond) Duration Fast Annular Lamp - Solid State Laser System. The segmented argon filled Annular Lamp is mounted between the Optical rail and the 12 unit - 5 K.V. - 3,000μF (48,000 joules max)capacitor bank. All high voltage points are enclosed by aluminum covers.

optical rails, the external mirror mounts, focusing optics and intercavity components.

The lamp itself was evacuated with a mechanical forepump and filled with argon gas to a pressure of 100 millimeters. The system was discharged by trigger transformers connected to the segmenting rings. After each discharge the system was purged with the mechanical fore pump and refilled with a fresh charge of argon gas.

The performance of the system is illustrated by the dual trace oscillogram shown in Figure 6-IIA showing on the upper trace the current through the lamp (sensitivity, 44 kiloamperes per major division) and on the lower trace the photoelectric record of the emission from a 0.58 x 8-inch long A.O. neodymium laser rod with TIR on one end and 55% dielectric coating on the other end. Horizontal sweep for both traces was 20 microseconds per major division. The integrated emission of the above neodymium laser rod as well as that of a 5/8-inch diameter x 8-inch long ruby with external 99% and 45% plane dielectric coated mirrors is shown in Figure 7-IIA. The laser system was seldom operated at capacitor bank loadings in excess of 30 kilojoules due to the high probability of rupture of the quartz segmenting rings.

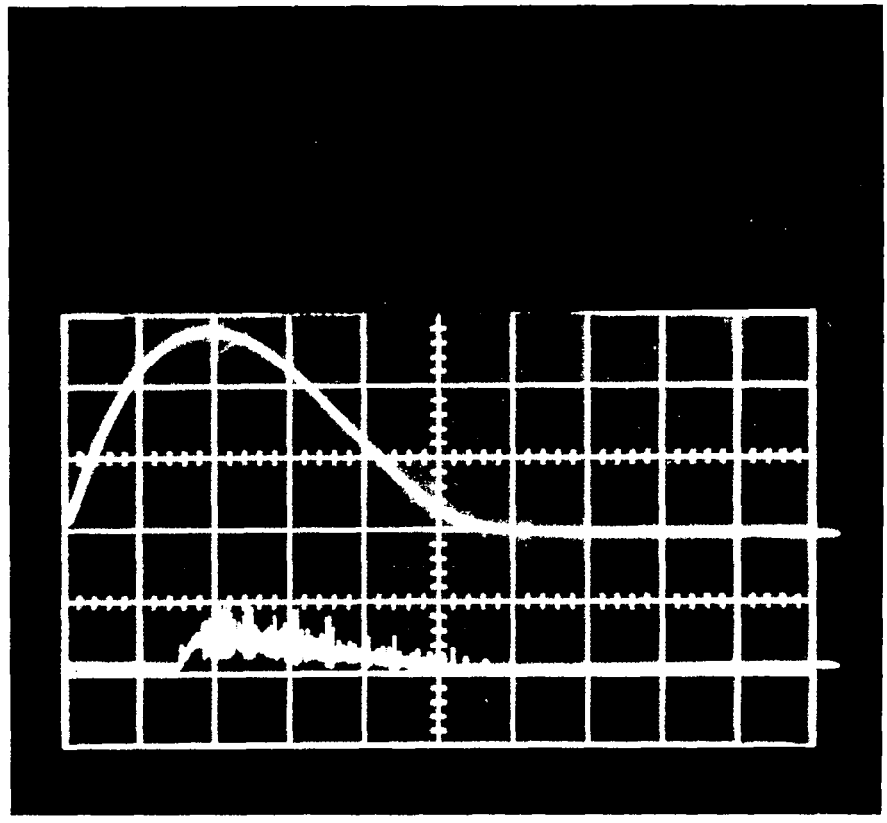

Figure 6-IIA: Dual Trace Oscillogram showing

Upper trace: current through segmented annular flash lamp at an initial bank energy of 18 kilojoules (vertical sensitivity; 44 kiloamperes per major scale division)

Lower trace: simultaneous emission from 0.58 x 8-inch A.O. neodymium doped laser rod with roof top on one end 55% coating on other end

Sweep speed: (both traces) 20 microseconds per major horizontal division

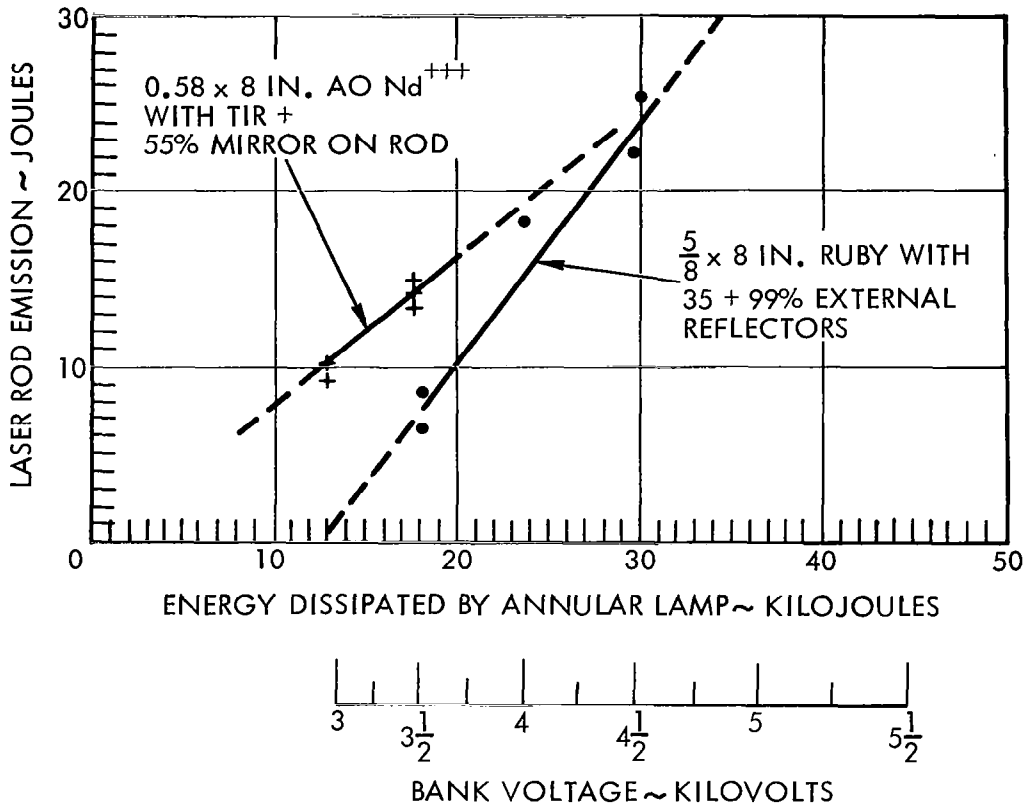

Figure 7-IIA: Performance of Intermediate Duration - Annular Lamp Laser with ruby and neodymium doped laser rods. Emission measured with TRG - ballistic thermopile.

The intermediate pulsed laser was used to make measurements of the effective exhaust velocity by using a vacuum mounted ballistic pendulum and "before and after" mass measurements with commercial high sensitivity balances.

The aiming telescope was attached to the optical rail along with the focusing objective (usually a 5 centimeter focal length simple lens). The small evacuated chamber (within which the test particles were mounted) was attached onto a commercial micromanipulator and the combination placed on a table before the focused laser beam. A close-up photograph of the vacuum chamber with its plexiglas windows and the holder with the focusing lens is shown in Figure 8-IIA. Also included is a picture of the vacuum plume from a piece of ferrite ablating under the 12 joule ~60 nanosecond duration focused beam from the 0.58 x 8-inch TIR neodymium doped laser rod. The ferrite block, in this case, lost approximately 1/2 milligram. The lack of sparks or cinders is a qualitative indication of low mass loss and accompanying high effective exhaust velocity. In comparison, tungsten ablated 1 milligram and a photograph of its plume showed sparks. Iron (drill rod) lost ~0.7 milligrams and, like tungsten, ablated macroscopic particles (sparks). Carbon (either pencil lead or pyrolitic graphite) had the highest impulse, the lowest mass loss (~0.2 milligrams), and thus the highest exhaust velocities (i.e., ~2-3 kilometer/second) of any material tested with the intermediate pulse laser. The preliminary studies indicated that the effective exhaust velocities with the intermediate laser were too low for acceleration to 20 kilometer/second meteoric velocities.

Work with the intermediate system was abandoned in favor of the Q-switched ruby laser system in order to determine effective exhaust velocities at ultimate power densities.

While the work with the Q-switch ruby was being conducted, the intermediate laser system was further refined into a "multiple-Giant Pulse" illuminator.* The intention here was to start the development of a laser which would emit a multiplicity of high peak power pulses in times proper to the acceleration of microparticles to hypervelocities.

Multiple giant pulsing of the intermediate duration laser was realized

*Conventional Q-switched lasers are essentially one-shot giant pulse emitters due to the limited brightness of the helical xenon flash lamp. The greater brightness of the segmented annular lamp made it possible to repump a laser rod to a high degree of inversion in times short compared to that of the conventional xenon lamp laser.

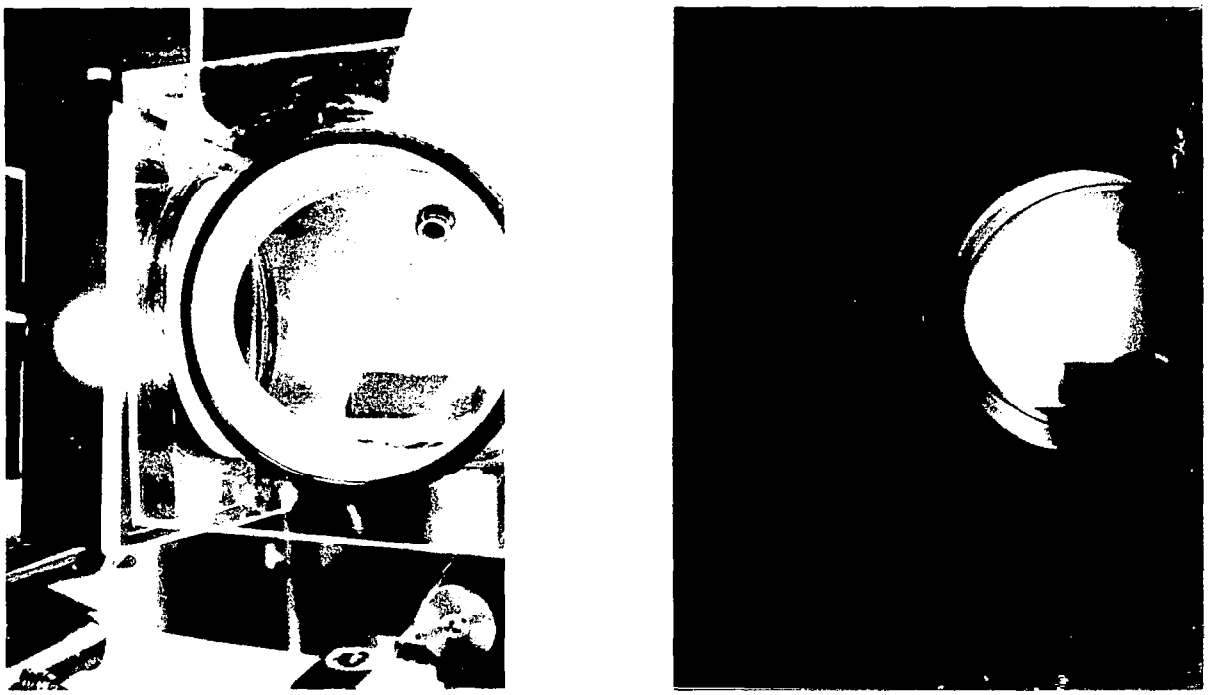

Figure 8-IIA: Photographs of the Vacuum Chamber mounted before the focusing lens attached to the rail of the intermediate pulse laser. A ferrite block was placed in the chamber and can be seen ablating under the 12 joules ~60 microsecond pulse from the neodymium laser. For the second photograph, the camera was set on bulb at f/22 with an N.D. 1 filter.

by replacing the neodymium doped glass laser rod by a 5/8 x 8-inch ruby rod,* and mounting external 99% and 45% plane dielectric coated reflectors at either end of the overhead optical rail. The end mirrors were separated by 1.2 meters. A 1/2-inch thick Beckman spectrophotometer cell filled with methanol and cryptocyanine was placed in the laser cavity before the 99% reflector.

The cryptocyanine cell is what is known as a bleachable shutter which "opens" when the gain of the laser rod exceeds the absorption of the dye. The cryptocyanine molecules are metastable and will remain in a non-absorbing state for times of the order of the laser's giant pulse. Cryptocyanine fulfills the same function as the polarizer and Kerr cell in a more conventional Giant pulse laser. Since it is automatic in its cycling, it does not require any of the electronic circuits, etc. of the electro-optical shutter.

By pumping the laser rod fast and adjusting the concentration of the dye in the cell, the magnitude and number of pulses can be determined.

An example of the multiple giant pulsing of the laser rod is shown in Figure 9-IIA. The oscillogram in this case was recorded with a photodiode driving 0.05μF ceramic capacitor in series with the 50Ω resistor terminating the photodiode circuit. The R-C termination was connected across the terminals of the Tektronix 555 oscilloscope. Each step in voltage on the oscillogram is proportional to the energy in the laser pulse. For the case shown, the laser emitted ten uniformly spaced giant pulses over an interval of 44 microseconds. The net energy emitted by the laser was ~9 joules (i.e., ~0.9 joules per pulse). For this measurement, the 3,000μF bank was charged to 4 K.V. (or 25,000 joules).

Unfortunately, the study terminated before any measurements of either impulse or mass loss were made with the multiply Q-switched intermediate duration laser. The unique operation of this laser is reported since it represents work done under the contract and illustrates that in addition to studying the interaction of laser radiation with material surfaces, basic work on laser sources was undertaken during this study.

---

*Product of Line Corporation, S.I.Q. grade ruby and not of particularly high optical homogeneity. Ruby was used (versus neodymium doped glass) in the initial experiments because of its capability to withstand higher peak optical power generated under Q switch conditions.

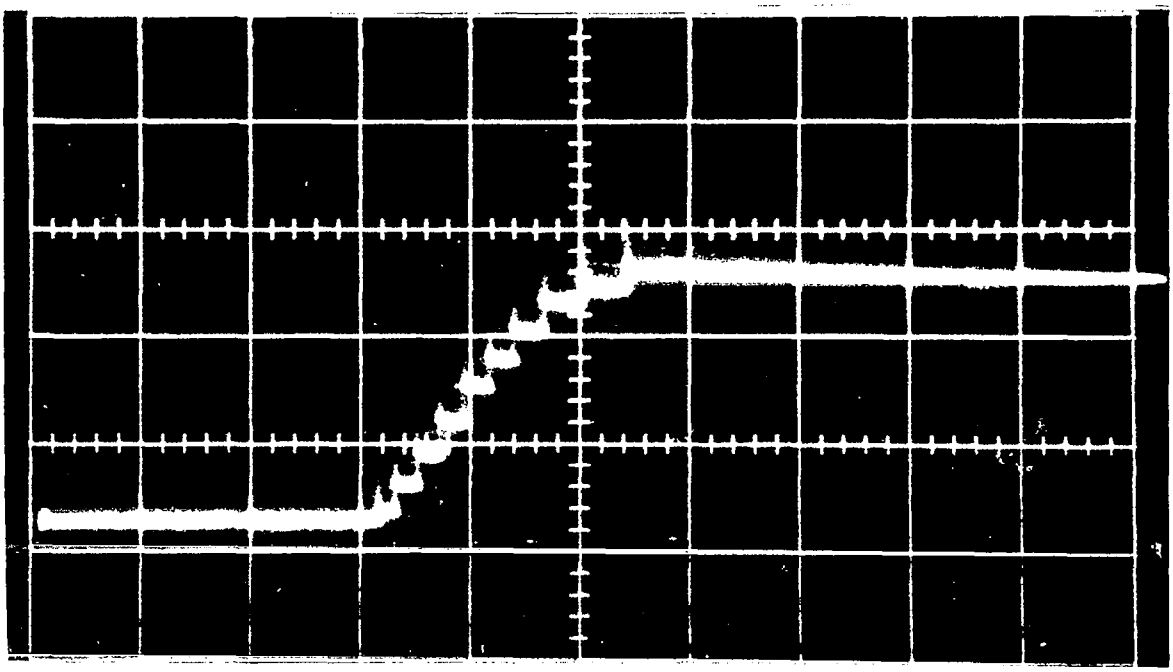

Figure 9-IIA: Integrated 9 joule emission from 5/8-inch diameter - 8-inch long ruby laser rod pumped by 24,000 joule discharge in the 50μsecond duration annular lamp. Vertical sensitivity ~4 joules/major division. Horizontal sensitivity, 20 μsec/ major division.

APPENDIX III

THEORY OF PARTICLE ACCELERATION BY EVAPORATION

This appendix is an unaltered copy of the first chapters of the original proposal for the feasibility study. It is included here because it states the background leading to the basic approach of the feasibility study, giving the reasons for the emphasis on "effective exhaust velocity."

I. THEORY OF PARTICLE ACCELERATION BY EVAPORATION

A. Introduction

There appear to be several possible methods by which one may attempt to accelerate small solid particles with laser energy. Perhaps the first scheme to come to mind is simply to impulsively vaporize matter from one side of a particle with a giant pulse laser. If the energy deposition time is assumed to be instantaneous and if the vaporized matter has mass M_v and is raised to a temperature T the gas will, upon expanding into a vacuum, give an impulse of $\{0.8\}\ \{M_v\}\ \sqrt{2C_vT}$ to the particle,* where C_v is the specific heat at constant volume. The final velocity of the particle is then given by

$$v_{final} = \frac{M_v}{M_{final}} \quad 0.8\ \sqrt{2\ C_vT} \quad .$$

Stating this result in terms of the total energy E absorbed from the laser we have

$$v_{final} = \frac{M_v}{M_{final}} \quad 0.8\ \sqrt{2\ \frac{E}{M_v}} \quad .$$

For a numerical example, we have that 1 joule absorbed in 10 percent of a 100 μ cube of carbon gives a final velocity about 8 km/sec. The corresponding temperature T is about 5×10^6 degrees K.

The effective time of acceleration, i.e., the time during which the major portion of the impulse is delivered to the particle, is approximately

$$2\ x_o\sqrt{\frac{M_v}{E}} \quad ,$$

*This is a one-dimensional approximation from K. P. Stanyukovich, Unsteady Motion of Continuous Media, Pergamon Press, New York, 1960, p. 157.

where X_o is the initial thickness of the vapor.* Thus the average acceleration force per unit area on the particle during this time is approximately

$$\frac{1}{3}\ \frac{E}{X_o A}\quad ,$$

where A is the area of the particle.

For the numerical example cited, the effective acceleration time is 3×10^{-10} sec and the acceleration pressure is 3×10^{12} nt/m^2. This time is shorter than the pulse from a giant pulse laser and the pressure is 3 orders of magnitude greater than the yield strength of steel. Moreover, since the acceleration time is short compared to the time a sound wave takes to cross the specimen, one can show that the energy content of the shock waves produced in the specimen contain more than enough energy to melt the final particle.

Several variations of the above scheme immediately come to mind. For example, partially absorbing coatings can be used on the particle so as to increase the thickness of the layer vaporized, thus increasing M_v. It appears, however, that 3 dimensional effects will invalidate the above formulas, should attempts be made to raise M_v/M_{final} even as far as 1.

Another simple variation of the above approach is to coat the particle with a layer of non-absorbing material. Then the vaporized layer will lie between the particle and the non-vaporized layer of non-absorbing material. The extreme in this direction is to stick the particle to a piece of glass (or quartz or diamond) and to focus the laser through the glass. The layer used to stick the particle to the glass can be of chosen thickness and proper absorbing properties so as to entirely vaporize.

It can readily be seen that here also, the

*Ibid.

accelerations are tremendous. For example, with a 100 μ cubical particle most of the acceleration must take place in a distance of 100 μ due to the fact that leakage of gas into 3-dimensional space sharply decreases the acceleration after this distance. For a 20 km/sec, 100 μ cube of density = 1, this acceleration pressure is still 2 orders of magnitude above the strength of steel. The acceleration time in this example is 10×10^{-9} sec which is slightly shorter than most giant pulse laser durations. There is thus some doubt as to whether one can deposit the required energy in the required time so that the explosive model is applicable. Moreover, in this example also, a severe consequence of the short acceleration period is the energy content of the shock waves within the particle. This energy can easily be sufficient to melt the particle or fracture it.

All the schemes mentioned thus far have in common, difficulties stemming from the extremely short length of the acceleration path. This short path requires acceleration pressures orders of magnitude greater than yield strengths, tremendous temperatures, and introduces sufficient energy into the final particle via shock waves to melt or vaporize the particle.

There appears to be at least two approaches which avoid these extremely short acceleration distances and, hence, avoid most of the problems mentioned above. The first is the use of a gun barrel to extend the acceleration path. In this approach energy can be fed in continuously during the acceleration process. The second is a rocket-like approach in which energy is continuously fed to ablate the tail of the particle and produce the exhaust gases.

The gun barrel approach appears to offer some promise and will be looked into should TRW/STL be awarded the study contract. The continuously-fed rocket approach looks

even more promising at this time and so the remaining portion of this section will be devoted to a moderately detailed examination of the rocket approach. As will be seen, a rather simple analysis coupled with some easily obtained experimental data allows the ultimate feasibility of the rocket approach to be determined.

B. The Basic Steady State Model

The rocket approach to particle acceleration, which circumvents many of the problems associated with extremely rapid acceleration, consists of ablating the tail of a particle at a controlled steady rate so that the particle itself behaves like a rocket. This model is readily susceptible to a preliminary analysis which will be given here.

Consider first, a given material in the form of a cylinder of diameter D in a vacuum. When laser radiation is incident on the end of this cylinder at a rate R per unit area, the temperature of the surface will rise until the vapor pressure of the material increases to the point where the energy carried away by the vaporized material is equal to the energy input. This process then can continue indefinitely at a steady state.

C. Remark on Departures from the Steady State Model

It is possible that the equilibrium just described is not a stable equilibrium, in which case, one would expect a pulsating rate of ablation. If this should be the case, much of the analysis to follow can be retained simply by taking time averages over the pulsation period. The same averaging process applies in the case of a spiking laser. Moreover, experiments have shown that, for some materials, droplets or solid pieces are thrown off along with the vapor. Here to, an averaging process allows much of the following theory to

be retained. The details of these averaging processes will be ignored in the following simple analysis.

D. Diffusion of Heat in the Specimen

A fact not immediately obvious in the above steady vaporization picture is that the diffusion of heat into the specimen does not act as a sink for energy. That is, the heat energy in the specimen is constant. We shall illustrate this fact with a one-dimensional analysis, some results of which will be useful later.

The heat equation may be written as

$$\frac{\partial T}{\partial t} = h^2 \frac{\partial^2 T}{\partial x^2}$$

where h^2 is the diffusivity of the material and x is the distance along the material. Let u denote the (constant) velocity with which the end of the cylinder is ablated. The position of the end is then given by $x = ut$. We now introduce a new coordinate system x_1 which moves with the ablating tail. The relation between the fixed and moving coordinate system is given by

$$x_1 = x - ut \quad .$$

When the heat equation is transformed to the moving coordinate system it becomes;

$$\frac{\partial T}{\partial t} - u \frac{\partial T}{\partial x_1} = h^2 \frac{\partial^2 T}{\partial x_1^2} \quad ,$$

which possesses the steady state solution

$$T(x_1, t) = T_o \, e^{-\frac{u}{h^2} x_1} \quad ,$$

where T_o is the temperature at the ablating surface $x_1 = 0$.

The total heat content per unit of cross section area inside the material is obtained by integrating and is given by

$$Q = T_o \frac{h^2}{u} \quad c\rho \quad ,$$

where c is the specific heat of the material and ρ is the density. Accordingly, one is led to the important conclusion that the heat content is <u>independent of time</u>. This means that conduction does not create a sink for energy.

Sixty-three percent of the heat specified in the previous equation is contained within the distance,

$$\frac{h^2}{u}$$

of the ablating surface. We shall refer to the quantity h^2/u as the diffusion distance. Note that as one would expect, the faster that one ablates the tail the less heat is contained in the material and the region where it is contained is thinner.

E. Details of the Vaporization Process

We return next to a more detailed description of the vaporization process. An estimate of the vapor pressure p of a given material as a function of surface temperature T can be obtained from the Clausius-Clapeyron equation.* This equation is of the form

$$p = P \exp(-T_2/T) \quad ,$$

where P and T_2 are constants for a given material. From the vapor pressure and surface temperature the rate of departure of molecules from the surface, per unit area, is given by

$$\frac{p}{\sqrt{2\pi\ kTm}} \quad ,$$

where m is the molecular weight and k is Boltzmann's constant. (Here the accommodation coefficient is taken to be =1). If one calculates the density just outside the surface due only to these departing molecules, one obtains

$$\frac{mp}{2\rho kT} \quad .$$

Here the density is given relative to the density ρ of the solid. If we evaluate these formulas, we find that even for graphite, which has a very low vapor pressure, the relative density is about 1/10 for a surface temperature of 8300°K. This means that the atoms are spaced only a little over twice as far apart as they are in the solid.

Such a high density will have two effects. First, the laser beam will be absorbed in the vapor rather than by the surface. The surface will be heated by conduction through the vapor and by radiation from the vapor. Secondly, there will be a large flux of molecules returning to the surface as

*It goes without saying that for each application it will be necessary to check the thermodynamic assumptions under which this equation was derived. In particular, one assumption which may be violated is that the ratio of solid density to vapor density be large.

a result of collisions in the high pressure vapor. The net flux of molecules will of course still be away from the surface, but may be much less than the flux of departing molecules.

The effective pressure Y on the surface causing the rocket to accelerate will be between p and 1/2 p, where p is the vapor pressure corresponding to the surface temperature T. If (as before) we denote by u the velocity, in the frame of the rocket, with which the tail of the rocket evaporates, we find that when the gas pressure just outside the surface is p, then u = 0. On the other hand, if none of the departing molecules are returned to the surface, then the velocity u would be given by

$$u_{max} = \frac{p}{\rho}\sqrt{\frac{m}{2\pi kT}} \quad .$$

The collision processes in the gas behind the rocket, together with the input of energy from the laser directly into this gas, result in an increase in the average velocity with which the gas molecules stream away from the rocket. Due to these processes, the effective exhaust velocity can be many times the molecular velocity associated with the surface temperature T. By the law of conservation of momentum, we can express this effective exhaust velocity v in terms of the effective acceleration pressure Y and the mass flow rate ρu. The result is

$$v = \frac{Y}{\rho u} \quad .$$

F. The Experimental Determination of Effective Exhaust Velocity and Ablation Rate

It should be noted that the effective exhaust velocity v is very easily measured in the laboratory, (even in the case where droplets or pieces are being expelled). To measure v one simply measures the total impulse to a given material by suspending the material as a ballistic pendulum

and observing its throw upon applications of a laser burst. This impulse is $Yt \frac{\pi}{4} D^2$, where t is the duration of the laser burst and D is the diameter of the specimen. Also measured before and after the shot is the mass of the specimen. The difference is the mass ablated which is $\rho ut \frac{\pi}{4} D^2$. The quotient of these quantities is v, the effective exhaust velocity. Also obtainable from the measured mass ablated, the known duration of the laser burst and specimen diameter is the velocity u with which the tail is ablated.

We, therefore, have the ability to determine both v and u by a very simple experiment. The parameters on which v and u depend will be: 1) the type of material, 2) the rate R per unit area at which the laser delivers energy, 3) the frequency (color) of the laser, and 4) the diameter D of the specimen. The diameter D enters as a parameter, for if the diameter is so small that the region in the exhaust gas where the main energy is absorbed is several diameters away from the tail, then three-dimensional effects will influence the efficiency with which the pressure created is conveyed to the rocket tail. In other words, some of the gas may be actually accelerated past the rocket in the forward direction.

G. Prediction of Rocket Performance From v and u

We shall now show how a knowledge of v and u enables one to predict the performance of the rocket and to intelligently optimize the remaining parameters at ones disposal.

We shall continue to assume that the rocket consists of a cylinder of diameter D with the laser ablating one end. Let L_1 denote the initial length of the cylinder and L_2 the final length of the cylinder at the end of the acceleration process. The well known rocket equation, obtained by integrating the equation expressing the conservation of momentum gives the final velocity V_{final} as

$$V_{final} = v \ln \frac{L_1}{L_2} \quad .$$

The acceleration time is the length ablated divided by the ablation velocity and may conveniently be written

$$t = \frac{L_2}{u} \left(\frac{L_1}{L_2} - 1 \right) \quad .$$

The acceleration distance is obtained by integrating the conservation of momentum equation twice with respect to time. The result is

$$x = L_2 \frac{v}{u} \left(\frac{L_1}{L_2} - \ln \frac{L_1}{L_2} - 1 \right) \quad .$$

The minimum power input from the laser, per unit area, is the acceleration pressure Y times the effective exhaust velocity v. This minimal power, per unit area R_m, can also be expressed as

$$R_m = \rho u v^2 \quad ,$$

since, as shown in E, $Y = \rho u v$. The actual rate R may be greater than this value depending on the nature of the three dimensional effects in the exhaust plume mentioned earlier. It would not be surpising to find that the minimal and actual rates are nearly the same for some materials.

The minimal total energy input is obtained by multiplying the above minimal rate times the time of acceleration and the area of the rocket. Thus

$$\text{minimal total energy input} = L_2 \rho v^2 \frac{\pi}{4} D^2 \left(\frac{L_1}{L_2} - 1 \right) .$$

Of course in the experiments performed to determine v and u the value of R, the actual power per unit area, will be known.

Thus, the scaling law for the actual energy input is

$$\text{actual total energy input} = L_2 \frac{R}{u} \frac{\pi}{4} D^2 \left(\frac{L_1}{L_2} - 1 \right) .$$

The efficiency of the rocket is the quotient obtained by dividing the final kinetic energy of the rocket by the total energy input. From the foregoing formulas, we obtain

$$\text{Efficiency} = \frac{R_m}{R} \left[\frac{(1/2) \ln^2 \frac{L_1}{L_2}}{\frac{L_1}{L_2} - 1} \right] .$$

The quantity in brackets has a very broad maximum of value 0.32 for $\frac{L_1}{L_2}$ approximately equal to 5. For $\frac{L_1}{L_2}$ in the range 1.7 to 30, the value of the term in brackets is greater than 0.20. We thus see that the need for efficiency does not put a tight restriction on the ratio $\frac{L_1}{L_2}$.

From the experimentally determined values of v and u, it is also instructive to compute the acceleration pressure Y;

$$Y = \rho v u .$$

This value may be compared directly to the yield strength of the material to obtain an idea of the stresses in the material, the state of the material and the energy stored in the material stresses.

The last application of the experimentally determined values of v and u is to estimate the thermal energy content of the final particle and hence to ascertain if the particle will be in the solid state. From the heat equation analysis given earlier, we found that the total heat content of the rocket material was $Q = T_o \frac{h^2}{u} CP$. This assumes that the diffusion distance h^2/u is less than the final

length L_2 of the rocket. When this heat is uniformly distributed over the final rocket, the final temperature will be

$$T_{final} = T_o \frac{h^2}{uL_2} \quad ,$$

where h^2, as before, is the diffusivity of the material. This formula assumes that there is no evaporation after the laser stops delivering power. This is not strictly true, but is a fair first approximation leading to too high an estimate of final temperature.

The temperature T_o of the surface can also be estimated from the experimentally derived values of v and u. This stems from the fact that the acceleration pressure Y is between 1/2p and p, where p is the vapor pressure. Since $Y = \rho vu$ we have

$$\rho vu < p < 2\rho vu \quad .$$

If we now employ the Clausius-Clapeyron equation for the vapor pressure $p = P \exp(-T_2/T)$, we obtain the bound

$$\frac{T_2}{\ln\left(\frac{P}{\rho vu}\right)} < T_o < \frac{T_2}{\ln\left(\frac{P}{2\rho vu}\right)} \quad ,$$

where P and T_2 are the vapor pressure constants for the material under consideration. For the present application, the two extremes of this inequality are essentially the same. Thus, we may write the following formula for the final temperature of the particle.

$$T_{final} = \frac{h^2}{uL_2} \quad \frac{T_2}{\ln\left(\frac{P}{2\rho vu}\right)} \quad .$$

H. Summary and Relation to the Experimental Program

In summary, we see that the foregoing scaling laws allow one to predict the performance of a laser particle accelerator from the experimentally determined values of v and u as functions of laser power density R, specimen diameter D, and type of material. From the given scaling laws, one may intelligently select the size of such parameters as L_2 and L_1/L_2 so that the acceleration process will achieve maximum final velocity for solid particles compatible with such factors as acceleration distance, strength of material, acceleration time (i.e., laser duration time), and laser energy available.

With these predictions at hand, the experimental program will then have a good background to work upon. The experimental program can then concentrate upon such problems as the stability of the angular position of the rocket and the stability of the tail ablation process. The first problem refers to the possibility of tumbling of the rocket. It will be necessary to determine if spinning, or mechanical constraining of the rocket is necessary. The problem of the stability of the ablation process is whether the shape of the ablation surface will remain flat or constant shape. It may, for example, become increasingly cone shaped if the laser beam is larger than the diameter of the particle, resulting in a diminishing thrust. On the other hand, a small laser beam can actually ablate a hole in the rocket. The experimental control of the energy density profile may be an important area of investigation.

The experimental program may then also consider variations of the basic scheme. For example, a variation worth considering is to make the rocket in the shape of a cone with the point in the direction of travel. Under certain conditions this geometry will permit a factor of 3 increase in final velocity due to the large increase in the initial to final mass ratio.

It is felt that the foregoing simple analysis will provide a background which will permit a rapid understanding and solution of the experimental problems.

I. Premature Numerical Estimates

It is obviously too early to make numerical evaluations of the potential for laser acceleration of small particles. Nevertheless, we shall make some guesses for a few of the parameters and illustrate the application of the preceeding formulas by working out the remaining parameters.

In the literature* there is some experimental evidence that exhaust velocities of 10 km/sec are possible for high rates of energy deposition. We shall thus select 10 km/sec as the effective exhaust velocity v for the example. In absence of knowledge of the ablation rate u we shall assume that the accelerating pressure is equal to the yield strength of steel, namely, 2×10^9 nt/m^2. For the material properties we shall use the values for graphite. The final length L_2 and particle diameter D will be assumed to be 100 μ and the ratio L_1/L_2 will be taken as 7 so that the final particle velocity will be 20 km/sec. With these assumptions we then obtain the following table of performance:

Assumptions	
Effective exhaust velocity v	10 km/sec
Acceleration pressure Y	2×10^9 nt/m^2
Final particle length L_2	100 μ
Particle diameter D	100 μ
Burn ratio L_1/L_2	7
Consequences	
Final velocity V_{final}	20 km/sec
Ablation velocity u	88 m/sec
Acceleration time t	7 μs
Acceleration distance	4.5 cm

*See References (3) and (4).

Diffusion distance h^2/u	1.4 μ
Surface temperature T_o	10,000°K
Final particle temperature T_{final}	140°C rise
Minimum total energy input	1.0 Joule

As a check on the possible contribution of acoustic or shock waves toward heating of the final particle we compare the distance sound travels in the acceleration time to the particle size. In this example sound travels 35 mm during the acceleration time. Thus, sound passes back and forth many times across the particle during the acceleration, resulting in the uniform acceleration of the particle with little energy contained in acoustic or shock waves.

"The aeronautical and space activities of the United States shall be conducted so as to contribute . . . to the expansion of human knowledge of phenomena in the atmosphere and space. The Administration shall provide for the widest practicable and appropriate dissemination of information concerning its activities and the results thereof."

—NATIONAL AERONAUTICS AND SPACE ACT OF 1958

NASA SCIENTIFIC AND TECHNICAL PUBLICATIONS

TECHNICAL REPORTS: Scientific and technical information considered important, complete, and a lasting contribution to existing knowledge.

TECHNICAL NOTES: Information less broad in scope but nevertheless of importance as a contribution to existing knowledge.

TECHNICAL MEMORANDUMS: Information receiving limited distribution because of preliminary data, security classification, or other reasons.

CONTRACTOR REPORTS: Scientific and technical information generated under a NASA contract or grant and considered an important contribution to existing knowledge.

TECHNICAL TRANSLATIONS: Information published in a foreign language considered to merit NASA distribution in English.

SPECIAL PUBLICATIONS: Information derived from or of value to NASA activities. Publications include conference proceedings, monographs, data compilations, handbooks, sourcebooks, and special bibliographies.

TECHNOLOGY UTILIZATION PUBLICATIONS: Information on technology used by NASA that may be of particular interest in commercial and other non-aerospace applications. Publications include Tech Briefs, Technology Utilization Reports and Notes, and Technology Surveys.

Details on the availability of these publications may be obtained from:

SCIENTIFIC AND TECHNICAL INFORMATION DIVISION

NATIONAL AERONAUTICS AND SPACE ADMINISTRATION

Washington, D.C. 20546